

# Predator Extinction arose from Chaos of the Prey: the Chaotic Behavior of a Homomorphic Two-Dimensional Logistic Map in the Form of Lotka-Volterra Equations

Wei Shan Lee\*, Hou Fai Chan, Ka Ian Im, Kuan Ieong Chan, and U Hin Cheang

Pui Ching Middle School Macau  
Macao Special Administrative Region, People's Republic of China.

## Abstract

A two-dimensional homomorphic logistic map that preserves features of the Lotka-Volterra equations was proposed. To examine chaos, iteration plots of the population, Lyapunov exponents calculated from Jacobian eigenvalues of the 2D logistic mapping, and from time series algorithms of Rosenstein and Eckmann et al. were calculated. Bifurcation diagrams may be divided into four categories depending on topological shapes. Our model not only recovered the 1D logistic map, which exhibits flip bifurcation, for the prey when there is a nonzero initial predator population, but it can also simulate normal competition between two species with equal initial populations. Despite the possibility for two species to go into chaos simultaneously, where the Neimark-Sacker bifurcation was observed, it is also possible that with the same interspecies parameters as normal but with a predator population 10 times more than that of the prey, the latter becomes chaotic, while the former dramatically reduces to zero with only a few iterations, indicating total annihilation of the predator species. Interpreting humans as predators and natural resources as preys in the ecological system, the above-mentioned conclusion may imply that not only excessive consumption of natural resources, but its chaotic state triggered by an overpopulation of humans may backfire in a manner of total extinction of the human species. Fortunately, there is little chance for the survival of the human race, as isolated fixed points in the bifurcation diagram of the predator reveal. Finally, two possible applications of the phenomenon of chaotic extinction are proposed: one is to inhibit viruses or pests by initiating the chaotic states of the prey on which the viruses or pests rely for existence, and the other is to achieve the superconducting state with the chaotic state of the applied magnetic field.

**Keywords** Flip Bifurcation, Neimark-Sacker Bifurcation, Logistic Map, Lyapunov Exponents, Lotka-Volterra Equations, Chaotic Extinction

## 1 Introduction

Understanding interactions between human beings and natural resources plays a vital role in the establishment of a sustainable economy and society. The prey and predator model may study the relationships of these two after we realize that humans may be regarded as predators. At the same time, natural resources may be considered preys[1]. Subsequently, research on prey-predator models can be implemented in this field instinctively[2]-[3].

Generally speaking, there are two main approaches of studies in the literature to this prey and predator model. The first is to study differential equations, while the other is to check the iterations in difference equations, whose forms may be inspired by directly applying the forward Euler scheme to acquire a counterpart of the former[4]-[10]. The discrete model could be more promising than the continuous one because it has more abundant dynamic characteristics in chaotic behaviors[8]. In contrast, it would be more difficult for solutions to continuous models to reach chaos in low-dimensional cases. Taking some examples of the first approach,

---

\*email: wslee@g.puiching.edu.mo

studies[11]-[12] have performed on the chaos of Lotka-Volterra differential equations with dimensions higher than three, and researchers[13] claimed that it is impossible to reach chaos for two species in the form of differential Lotka-Volterra equations, whose general solutions were obtained in sinusoidal forms by Evans and Findley[14]. Additionally, based on the Lotka-Volterra model, Dunbar[15] confirmed the existence of traveling wave solutions for two reaction-diffusion systems. In addition to that, Das and Gupta[16] proposed solutions to the fractional-order time derivative Lotka-Volterra equations using an analytical approach for nonlinear problems known as the homotopy perturbation method (HPM).

In addition, there are also several studies on the discrete difference equations. For example, Bessoir and Wolf [17] made pioneering contributions to the application of 1D logistic equation on biological and ecological studies. Many researchers also used the same equation to interpret, analyze and predict data according to COVID-19[18]. Mareno and English[19] implemented the 1D logistic equation to the coupled 2D logistic, and demonstrated that for a high growth rate the system underwent a Neimark-Sacker bifurcation. Li et al.[20] imposed an equal intensity of individual effects, corresponding to the same growth rate in the 1D logistic map, on the two oligopolists in the homomorphic Kopel model and observed three different kinds of bifurcation. Furthermore, Elhadi and Sprott[21] proposed a two-dimensional mapping, one of which is the ordinary 1D logistic map, while the other consists of a perturbation term of the former and is also modulated by the first. Shilnikov and Rulkov[22] studied chaos behaviors in two-dimensional difference equations that reproduced spike bursting activities in biological neurons, further improving previous research based on the three-dimensional system of ODEs. Despite applying the forward Euler scheme to acquire the difference equation, researchers also used exponential forms corresponding to solutions in the differential equations. For example, Ishaque et al.[23] studied a three-dimensional predator-prey-parasite model with an exponential form that describes interactions between healthy or infected Tilapia fish as prey and Pelican birds as predator. Tassaddiq et al.[24] worked on the discrete-time exponential difference equation of the Leslie-Gower predator-prey model together with a Holling type III functional response and indicated the advantage in this type of discretization method. A previous study[25] suggested a heteromorphic term that describes the decreasing effects on the predator that was only linear to the population of that species, contrary to the corresponding quadratic term in the prey. Hassell et al.[26] applied the predator-prey model to insect parasitoids and anthropods, and found that local movements of the two species may cause the extermination of the entire ecological system with chaos, and it is difficult to maintain population stability for a large growth rate of anthropods. Furthermore, researchers[27] also noted that human misbehavior may be the reason why an ecological system goes into chaotic states, and Danca et al.[28] studied predator extinction behavior after long iterations and provided solutions to prevent it from happening. Unfortunately, their system cannot see extinction directly in the bifurcation diagram due to the asymmetric form in their evolution equation.

However, there is no convincing reason for prey and predator to have different forms in the difference equations. Intuition in mathematical symmetry naturally came to our mind that a successful predator-prey difference model should resemble the symmetry structure as in the Lotka-Volterra differential equations. Moreover, solutions to Lotka-Volterra equations in sinusoidal forms cannot explain the extinction of species.

We proposed homomorphic two-dimensional logistic maps that preserve both forms of the Lotka-Volterra Equations and the 1D logistic equation. In our model, we conjectured a quadratic form in both the corresponding terms of the prey and the predator, treating both species on the equal stance. The structures of the bifurcation diagrams showed that there could be four different categories in our dynamic system. For each category, we examined population iterations, phase portraits, phase space diagrams, and topological types of fixed points. Lyapunov exponents calculated from Jacobian eigenvalues of the 2D mapping or from time-series algorithms, either Rosenstein[29] or Eckmann et al.[30], were also calculated. Comparisons among those results were also discussed.

The advantages of our model include the following. First, we may be able to establish a standard bifurcation diagram of 1D logistic map about the prey with a non-zero initial predator population, growth rates in both species, and predation parameters. Second, our model may also describe the normal behavior of the rise and fall in the population of the two species when they interact with each other. Third, in addition to simultaneous chaos in both species, the main discovery in our research was that the predator may go extinct under the circumstance of chaos in the prey for which the predator overpopulation should be blamed.

## 2 Model Formulation

We first review the one-dimensional logistic equation and the two-dimensional Lotka-Volterra equations, comparing the similarities and differences between the two sets of equations. This inspires us to construct two hypotheses to establish our two-dimensional logistic equations that maintain the essential features of the original ones.

### 2.1 Hypotheses inspired from 1D logistic equation and Lotka-Volterra Equations

To begin with, the one-dimensional logistic equation may be written as

$$x_{n+1} = \mu_0 x_n (1 - x_n), \quad (1)$$

where  $\mu_0$  denotes to the growth rate.

On the other hand, the two-dimensional Lotka-Volterra equations[31], [32] describe interactions between prey and predator in an environment where there is sufficient food supply for the prey, whose only natural enemy is the predator. The formula may be written as follows:

$$\begin{cases} \frac{dx}{dt} = \mu_0 x - \mu_1 xy; \\ \frac{dy}{dt} = -\nu_0 y + \nu_1 xy, \end{cases} \quad (2a)$$

$$\quad (2b)$$

where  $\mu_0$ ,  $\mu_1$ ,  $\nu_0$ , and  $\nu_1$  are all positive parameters.  $x$  denotes the prey population, while  $y$  is the predator population, both belong to  $[0, 1]$ .  $\mu_0$  is the (per capita) growth rate of the prey, and  $\mu_1$  refers to the inter-species parameter for the prey in the presence of the predator.  $\nu_0$  refers to the (per capita) death rate, resulting from all effects that decrease the population of the predator, which may include disease, death, or emigration[33]. At last,  $\nu_1$  refers to the (per capita) growth rate of the predator at the presence of the prey.

With forward Euler's scheme, one may immediately write the difference version of Eq.(2) as follows

$$\begin{cases} x_{n+1} - x_n = \mu_0 x_n - \mu_1 x_n y_n; \\ y_{n+1} - y_n = -\nu_0 y_n + \nu_1 x_n y_n. \end{cases} \quad (3a)$$

$$\quad (3b)$$

However, there is an obvious drawback about the above simultaneous equations: it does not preserve the feature of 1D logistic equation because the first term on the right-hand side is linear to either  $x_n$  or  $y_n$ , while the right-hand side in Eq.(1) is quadratic to  $x_n$ .

We now discuss establishing a two-dimensional map that resembles the interaction terms of the prey and the predator, as in Lotka-Volterra. First, we may rewrite the linear term of  $x$  on the right-hand side of Eq.(2a) into quadratic, which looks like  $\mu_0 x(1 - x)$ , together with the homomorphic corresponding term in Eq.(2b) as  $\nu_0 y(1 - y)$ . Thus, the modified Lotka-Volterra Equations[34] are

$$\begin{cases} \frac{dx}{dt} = \mu_0 x(1 - x) - \mu_1 xy; \\ \frac{dy}{dt} = -\nu_0 y(1 - y) + \nu_1 xy, \end{cases} \quad (4a)$$

$$\quad (4b)$$

whose resemblance in the form of difference equations is, therefore,

$$\begin{cases} x_{n+1} - x_n = \mu_0 x_n(1 - x_n) - \mu_1 x_n y_n; \\ y_{n+1} - y_n = -\nu_0 y_n(1 - y_n) + \nu_1 x_n y_n. \end{cases} \quad (5a)$$

$$\quad (5b)$$

Although it seems more reasonable to the direct resemblance of Lotka-Volterra Equations, Eq.(5) (Type 1) fails to restore Eq.(1) when parameters other than  $\mu_0$  are all set to zero. Fortunately, we may modify this by dropping  $x_n$  and  $y_n$  terms on the left-hand side of the above equations

$$\begin{cases} x_{n+1} = \mu_0 x_n(1 - x_n) - \mu_1 x_n y_n; \\ y_{n+1} = -\nu_0 y_n(1 - y_n) + \nu_1 x_n y_n, \end{cases} \quad (6a)$$

$$\quad (6b)$$

which is the desired form. On the basis of the above discussions, we state the following two hypotheses:

**Hypothesis H<sub>1</sub>:** The mathematical formulation of the population is the *same* for every species in the ecological system. This is also an intuition for mathematical symmetry.

**Hypothesis H<sub>2</sub>:** The predation of the prey in the presence of the predator (interspecies constant), death rate and growth rate of the predator are *all* proportional to the growth rate of the prey with different proportionality.

Since Eq.(5) and Eq.(6) both satisfy Hypotheses H<sub>1</sub> and H<sub>2</sub>, we divide into two cases to further study the properties of Eq.(5) (Type 1) and Eq.(6) (Type 2) in Sect. 2.3 and Sect. 2.4. But before that, in the next subsection, we first discuss a fundamental lemma that allows us to study the stability behaviors of fixed points.

## 2.2 Stability of fixed points

Suppose that a mapping of two-dimensional iterations  $x_{n+1}$  and  $y_{n+1}$  is written as  $x_{n+1} = f(x_n, y_n)$  and  $y_{n+1} = g(x_n, y_n)$ . The Jacobian is, therefore,

$$\begin{cases} J = \frac{\partial(f, g)}{\partial(x, y)} & (7a) \\ = \begin{pmatrix} \frac{\partial f}{\partial x} & \frac{\partial f}{\partial y} \\ \frac{\partial g}{\partial x} & \frac{\partial g}{\partial y} \end{pmatrix}, & (7b) \end{cases}$$

whose eigenvalues are  $\omega_0$  and  $\omega_1$ . It is well known[6], [8] that a fixed point can be divided into the following four topological types according to their stability behaviors. First, it could be a *sink* and locally asymptotic stable if eigenvalues of Eq.(7) satisfy  $|\omega_0| < 1$  and  $|\omega_1| < 1$ . Second, it could be a *source* and locally unstable if the eigenvalues satisfy  $|\omega_0| > 1$  and  $|\omega_1| > 1$ . Third, a fixed point could be a *saddle* if one of the absolute values of the eigenvalues is greater than 1 while the other is smaller than 1. Finally, a fixed point could be *non-hyperbolic* if one of the absolute values of the eigenvalues is equal to 1. The stability of a non-hyperbolic fixed point is fragile[35], which means that the small nonlinear terms easily influence its stability.

Instead of directly calculating the range of eigenvalues, most of the time it is more convenient to work with the quadratic formula consisting of eigenvalues  $\omega_0$  and  $\omega_1$ , namely,  $\Omega(\omega) = \omega^2 - \text{Tr}(J)\omega + \det(J)$ , where  $\text{Tr}(J)$  and  $\det(J)$  are trace and determinant of Jacobian in Eq.(7), respectively, and there could be a correspondence on the stability behavior around a fixed point between the roots of the quadratic formula,  $\omega_0$  and  $\omega_1$ , which are also Jacobian eigenvalues, through the following Lemma[8]

**Lemma 1.** *Let  $\Omega(\omega) = \omega^2 - \text{Tr}(J)\omega + \det(J)$ , be a quadratic formula where  $\text{Tr}(J)$  and  $\det(J)$  are trace and determinant of Jacobian in Eq.(7), respectively. Then*

1. *If  $\Omega(1) > 0$ , then*

- (a)  *$|\omega_0| < 1$  and  $|\omega_1| < 1$  and hence the fixed point is a sink if and only if  $\Omega(-1) > 0$  and  $\det(J) < 1$ ;*
- (b)  *$|\omega_0| > 1$  and  $|\omega_1| > 1$  and therefore the fixed point is a source if and only if  $\Omega(-1) > 0$  and  $\det(J) > 1$ ;*
- (c) *One of  $|\omega_0|$  and  $|\omega_1|$  is smaller than 1 while the other greater than 1 and hence the fixed point is a saddle if and only if  $\Omega(-1) < 0$ ;*
- (d) *Either  $|\omega_0|$  or  $|\omega_1|$  is equal to 1 and hence the fixed point is a non-hyperbolic whenever*
  - i.  *$\omega_0 = -1$  and  $\omega_1 \neq -1$  if and only if  $\Omega(-1) = 0$  and  $\text{Tr}(J) \neq 2$ .*
  - ii.  *$\omega_0$  and  $\omega_1$  are a pair of complex conjugates and  $|\omega_0| = |\omega_1| = 1$  if and only if  $|\text{Tr}(J)| < 2$  and  $\det(J) = 1$ .*
  - iii.  *$\omega_0 = \omega_1 = -1$  if and only if  $\Omega(-1) = 0$  and  $\text{Tr}(J) = 2$ .*

2. *If  $\Omega(1) = 0$ , then either  $|\omega_0|$  or  $|\omega_1|$  has to be equal to 1. Therefore, the fixed point is a non-hyperbolic. The absolute value of the other root is greater than, equal to, or smaller than 1 if and only if; correspondingly, the absolute value of  $\det(J)$  is greater than, equal to, or smaller than 1.*



3. If  $\Omega(1) < 0$ , then either  $|\omega_0|$  or  $|\omega_1|$  must be greater than 1. Therefore, the fixed point is a saddle. Also,
- (a) the other root is smaller or equal to  $-1$  if and only if, correspondingly,  $\Omega(-1) < -1$  or  $\Omega(-1) = -1$ .
  - (b) absolute value of the other root is less than 1 if and only if  $\Omega(-1) > 0$ .

Lemma 1 makes it easier for us to study the stability of fixed points analytically. In our analysis, we omitted all cases with negative parameters, as well as  $\mu_0 < 1$ .

### 2.3 Properties of Eq.(5) (Type 1)

Setting up  $x_{n+1} = f(x_{n+1}, y_{n+1})$  and  $y_{n+1} = g(x_{n+1}, y_{n+1})$ , the two-dimensional logistic equations in Eq.(5) (Type 1) have the mappings

$$\begin{cases} f(x, y) = \mu_0 x(1 - x) - \mu_1 xy + x; & (8a) \\ g(x, y) = -\nu_0 y(1 - y) + \nu_1 xy + y. & (8b) \end{cases}$$

Eq.(8) has Jacobian, as indicated in Eq.(7),

$$J = \begin{pmatrix} \mu_0(1 - 2x) - \mu_1 y + 1 & -\mu_1 x \\ \nu_1 y & \nu_0(-1 + 2y) + \nu_1 x + 1 \end{pmatrix}, \quad (9)$$

with eigenvalues  $\omega_0$  and  $\omega_1$  being, respectively,

$$\begin{cases} \omega_0 = -\mu_0 x + \nu_0 y + 1 + \frac{1}{2}(x\nu_1 - y\mu_1) + \frac{1}{2}(\mu_0 - \nu_0) + \frac{\omega}{2} & (10a) \\ \omega_1 = -\mu_0 x + \nu_0 y + 1 + \frac{1}{2}(x\nu_1 - y\mu_1) + \frac{1}{2}(\mu_0 - \nu_0) - \frac{\omega}{2} & (10b) \end{cases}$$

where

$$\begin{aligned} \omega = & \left[ 4\left(\nu_0 + \frac{\mu_1}{2}\right)^2 y^2 + \left( \left( (4\mu_0 - 2\nu_1)\mu_1 + 8\nu_0\left(\mu_0 + \frac{\nu_1}{2}\right) \right) x - 4(\nu_0 + \mu_0)\left(\nu_0 + \frac{\mu_1}{2}\right) \right) y \right. \\ & \left. + 4\left( \left(\mu_0 + \frac{\nu_1}{2}\right)x - \frac{\mu_0}{2} - \frac{\nu_0}{2} \right)^2 \right]^{\frac{1}{2}} \end{aligned} \quad (11)$$

Further, fixed points, at which pairs of  $x$  and  $y$  stay still irrespective of time-series iterations[35], are those pairs of points  $(x^*, y^*)$  such that

$$\begin{cases} x^* = \mu_0 x^*(1 - x^*) - \mu_1 x^* y^* + x^* & (12a) \\ y^* = \nu_0 y^*(1 - y^*) - \nu_1 x^* y^* + y^*, & (12b) \end{cases}$$

from which four pairs of fixed points  $(x^*, y^*)$  may be derived as

$$\begin{cases} E_0 = (0, 0) & (13a) \\ E_1 = (0, 1) & (13b) \\ E_2 = (1, 0) & (13c) \\ E_3 = \left( \frac{\nu_0(\mu_1 - \mu_0)}{-\mu_0\nu_0 + \mu_1\nu_1}, \frac{\mu_0(\nu_1 - \nu_0)}{-\mu_0\nu_0 + \mu_1\nu_1} \right), & (13d) \end{cases}$$

provided that the denominator in Eq.(13d) is not zero. On the contrary, however, when  $\mu_0\nu_0 = \mu_1\nu_1$ , Eq.(5) (Type 1) has fixed points  $E_0, E_1,$ and  $E_2$ .

Keeping **Lemma 1** in Sect. 2.2 in mind, we may be able to examine the topological type of each fixed point in Eq.(13) as in Theorem 1:

**Theorem 1.** *The topological types of fixed points in Eq.(13) are*

1. For  $E_0 = (0, 0)$ ,

$$\begin{cases} \Omega(1) = -\mu_0\nu_0 \\ \Omega(-1) = (2 + \mu_0)(2 - \nu_0) \\ \det(J) = (1 + \mu_0)(1 - \nu_0) \\ \text{Tr}(J) = 2 + \mu_0 - \nu_0. \end{cases}$$

Because  $\Omega(1) < 0$ ,  $E_0$  is always a saddle.

2. For  $E_1 = (0, 1)$ ,

$$\begin{cases} \Omega(1) = \nu_0(\mu_0 - \mu_1) \\ \Omega(-1) = (2 + \nu_0)(2 + \mu_0 - \mu_1) \\ \det(J) = (1 + \nu_0)(1 + \mu_0 - \mu_1) \\ \text{Tr}(J) = 2 + \mu_0 - \mu_1 + \nu_0. \end{cases}$$

Therefore,

- (a) the fixed point is a source if  $\mu_0 > \mu_1$
- (b) the fixed point is a saddle if  $\mu_0 < \mu_1$ .
- (c) the fixed point is a non-hyperbole if  $\mu_0 = \mu_1$

3. For  $E_2 = (1, 0)$ ,

$$\begin{cases} \Omega(1) = -\mu_0(\nu_1 - \nu_0) \\ \Omega(-1) = (2 - \mu_0)(2 + \nu_1 - \nu_0) \\ \det(J) = (1 - \mu_0)(1 + \nu_1 - \nu_0) \\ \text{Tr}(J) = 2 - \mu_0 + (\nu_1 - \nu_0). \end{cases}$$

In this case,

- (a) the fixed point is a sink if one of the following sustains:
  - i.  $\mu_0 < 2$ , and  $\nu_1 < \nu_0 < \nu_1 + 1$
  - ii.  $\mu_0 < 2$ , and  $\nu_0 = \nu_1 + 1$
  - iii.  $\mu_0 < 2$ , and  $\nu_1 + 1 < \nu_0 < \nu_1 + 2$
- (b) if  $\mu_0 > 2$  and  $\nu_0 > \nu_1 + 2$ , then  $E_2$  is a source;
- (c) the fixed point is a saddle if one of the following sustains:
  - i.  $\mu_0 > 2$  and  $\nu_1 < \nu_0 < \nu_1 + 2$
  - ii.  $\mu_0 < 2$  and  $\nu_0 > \nu_1 + 2$
  - iii.  $\nu_0 < \nu_1$
- (d) the fixed point is a non-hyperbole because of Lemma 1-1(d) if one of the following sustains:
  - i.  $\mu_0 = 2$  and  $\nu_1 < \nu_0 < \nu_1 + 2$
  - ii.  $\mu_0 \leq 2$ ,  $\nu_0 = \nu_1 + 2$
  - iii.  $\mu_0 > 2$  and  $\nu_0 = \nu_1 + 2$
  - iv.  $\mu_0 = 2$  and  $\nu_0 > \nu_1 + 2$

4. For  $E_3 = \left( \frac{\nu_0(\mu_1 - \mu_0)}{-\mu_0\nu_0 + \mu_1\nu_1}, \frac{\mu_0(\nu_1 - \nu_0)}{-\mu_0\nu_0 + \mu_1\nu_1} \right)$ ,

$$\begin{cases} \Omega(1) = -\frac{\mu_0\nu_0(\nu_0 - \nu_1)(\mu_0 - \mu_1)}{\mu_0\nu_0 - \mu_1\nu_1} \\ \Omega(-1) = \frac{-\nu_0(\nu_0 - \nu_1 + 2)\mu_0^2 + \nu_0(\mu_1 + 2)(\nu_0 - \nu_1 + 2)\mu_0 - 4\mu_1\nu_1}{\mu_0\nu_0 - \mu_1\nu_1} \\ \det(J) = \frac{-\nu_0(\nu_0 - \nu_1 + 1)\mu_0^2 + \nu_0(\mu_1 + 1)(\nu_0 - \nu_1 + 1)\mu_0 - \mu_1\nu_1}{\mu_0\nu_0 - \mu_1\nu_1} \\ \text{Tr}(J) = \frac{-\mu_0^2\nu_0 + \nu_0(\nu_0 + \mu_1 - \nu_1 + 2)\mu_0 - 2\mu_1\nu_1}{\mu_0\nu_0 - \mu_1\nu_1}. \end{cases}$$

There are a lot of combinations for criteria of a sink from **Lemma 1-1(a)**, a source from **Lemma 1-1(b)**, and a saddle from **Lemma 1-1(c)**. We only provide conditions for a saddle from **Lemma 1-3** and a non-hyperbole.

(a) the fixed point is a saddle because of **Lemma 1-3** if one of the following holds:

- i.  $\mu_0 = 1, \mu_1 < 1, \nu_1 < \nu_0$ , and  $\frac{\nu_0}{\nu_1} < \mu_1$
- ii.  $\mu_0 = 1, \nu_1 < \nu_0$ , and  $\frac{\nu_0}{\nu_1} < \mu_1$
- iii.  $\mu_0 = 1, \mu_1 < 1, \nu_0 < \nu_1$ , and  $\frac{\nu_0}{\nu_1} < \mu_1$
- iv.  $\mu_0 > 1, \mu_1 < \mu_0$ , and  $\nu_1 < \nu_0$
- v.  $\mu_0 > 1, \nu_1 < \nu_0$ , and  $\frac{\mu_0\nu_0}{\nu_1} < \mu_1$
- vi.  $\mu_0 > 1, \mu_1 < \mu_0, \nu_0 < \nu_1$ , and  $\frac{\mu_0\nu_0}{\nu_1} < \mu_1$

(b) the fixed points is a non-hyperbole because of **Lemma 1-2** if one of the following holds:

- i.  $\mu_0 = 1, \mu_1 = 1$ , and  $\nu_1 < \nu_0$
- ii.  $\mu_0 = 1$ , and  $\mu_1 \leq 1$
- iii.  $\mu_0 = 1, \nu_1 = \nu_0$ , and  $\mu_1 > 1$
- iv.  $\mu_0 = 1, \mu_1 = 1$ , and  $\nu_0 < \nu_1$
- v.  $\mu_1 = \mu_0, \mu_0 > 1$ , and  $\nu_1 < \nu_0$
- vi.  $\nu_1 = \nu_0, \mu_0 > 1$ , and  $\mu_1 < \mu_0$
- vii.  $\mu_1 = \mu_0, \nu_1 = \nu_0$ , and  $\mu_0 > 1$
- viii.  $\nu_1 = \nu_0, \mu_0 > 1$ , and  $\mu_0 < \mu_1$
- ix.  $\mu_1 = \mu_0, \mu_0 > 1$ , and  $\nu_0 < \nu_1$

(c) the fixed points is a non-hyperbole because of **Lemma 1-1(d)** if one of the following holds:

- i.  $\mu_0 = 1, \mu_1 = -\frac{\nu_0(-\nu_1+\nu_0+2)}{\nu_0^2-\nu_1\nu_0+2\nu_0-4\nu_1}, \nu_0 < 2, \nu_0 < \nu_1$ , and  $\nu_1 < \nu_0 + 2$
- ii.  $\mu_1 = \frac{\mu_0\nu_0(\mu_0\nu_0-\mu_0\nu_1+2\mu_0-2\nu_0+2\nu_1-4)}{\mu_0\nu_0^2-\nu_1\mu_0\nu_0+2\mu_0\nu_0-4\nu_1}, 1 < \mu_0 < 2, \nu_0 < 2, \nu_0 < \nu_1$ , and  $\nu_1 < \nu_0 + 2$
- iii.  $\mu_1 = \frac{\mu_0\nu_0(\mu_0\nu_0-\mu_0\nu_1+2\mu_0-2\nu_0+2\nu_1-4)}{\mu_0\nu_0^2-\nu_1\mu_0\nu_0+2\mu_0\nu_0-4\nu_1}, \mu_0 > 2, \nu_0 < 2, \nu_0 < \nu_1$ , and  $\nu_1 < \frac{\mu_0\nu_0(\nu_0+2)}{\mu_0\nu_0+4}$
- iv.  $\mu_1 = \frac{\mu_0\nu_0(\mu_0\nu_0-\mu_0\nu_1+2\mu_0-2\nu_0+2\nu_1-4)}{\mu_0\nu_0^2-\nu_1\mu_0\nu_0+2\mu_0\nu_0-4\nu_1}, \mu_0 > 2, \mu_0 > 2, \nu_0 < 2, \nu_1 < \frac{\mu_0(\nu_0+2)}{\mu_0-2}$ , and  $\nu_0 + 2 < \nu_1$
- v.  $\mu_0 = 1, \mu_1 = -\frac{\nu_1-4}{3\nu_1-4}, \nu_0 = 2$ , and  $2 < \nu_1 < 4$
- vi.  $\mu_1 = \frac{\mu_0(\mu_0\nu_1-4\mu_0-2\nu_1+8)}{\mu_0\nu_1-4\mu_0+2\nu_1}, \nu_0 = 2, 1 < \mu_0 < 2$ , and  $2 < \nu_1 < 4$
- vii.  $\mu_1 = \frac{\mu_0(\mu_0\nu_1-4\mu_0-2\nu_1+8)}{\mu_0\nu_1-4\mu_0+2\nu_1}, \nu_0 = 2, \mu_0 > 2$ , and  $2 < \nu_1 < \frac{4\mu_0}{\mu_0+2}$
- viii.  $\mu_1 = \frac{\mu_0(\mu_0\nu_1-4\mu_0-2\nu_1+8)}{\mu_0\nu_1-4\mu_0+2\nu_1}, \nu_0 = 2, \mu_0 > 2$ , and  $4 < \nu_1 < \frac{4\mu_0}{\mu_0-2}$
- ix.  $\mu_1 = 1, \mu_1 = -\frac{\nu_0(-\nu_1+\nu_0+2)}{\nu_0^2-\nu_1\nu_0+2\nu_0-4\nu_1}$ , and  $2 < \nu_0 < \nu_1 < \nu_0 + 2$
- x.  $\mu_1 = \frac{\mu_0\nu_0(\mu_0\nu_0-\mu_0\nu_1+2\mu_0-2\nu_0+2\nu_1-4)}{\mu_0\nu_0^2-\nu_1\mu_0\nu_0+2\mu_0\nu_0-4\nu_1}, 1 < \mu_0 < 2$ , and  $2 < \nu_0 < \nu_1 < \nu_0 + 2$
- xi.  $\mu_1 = \frac{\mu_0\nu_0(\mu_0\nu_0-\mu_0\nu_1+2\mu_0-2\nu_0+2\nu_1-4)}{\mu_0\nu_0^2-\nu_1\mu_0\nu_0+2\mu_0\nu_0-4\nu_1}, 2 < \mu_0$ , and  $2 < \nu_0 < \nu_1 < \frac{\mu_0\nu_0(\nu_0+2)}{\mu_0\nu_0+4}$
- xii.  $\mu_1 = \frac{\mu_0\nu_0(\mu_0\nu_0-\mu_0\nu_1+2\mu_0-2\nu_0+2\nu_1-4)}{\mu_0\nu_0^2-\nu_1\mu_0\nu_0+2\mu_0\nu_0-4\nu_1}, 2 < \mu_0, 2 < \nu_0$ , and  $\nu_0 + 2 < \nu_1 < \frac{\mu_0(\nu_0+2)}{\mu_0-2}$

By Hypothesis H<sub>2</sub>, we further assume proportionality of parameters  $\mu_1 = \alpha\mu_0, \nu_0 = \beta\mu_0$ , and  $\nu_1 = \gamma\mu_0$ , where  $\alpha, \beta$ , and  $\gamma$  are other designated parameters. Under this circumstance, the nontrivial fixed point  $E_3$  becomes

$$E_3 = \left( \frac{\beta(\alpha-1)}{\alpha\gamma-\beta}, \frac{\gamma-\beta}{\alpha\gamma-\beta} \right),$$

which is independent of the growth rate parameter  $\mu_0$ . It should be noted that for  $E_3$  to remain inside the square enclosed by the vortexes  $(0,0), (0,1), (1,1), (1,0)$ ,  $\alpha, \beta$ , and  $\gamma$  must satisfy either  $\{\alpha < 1, \text{ and } \gamma < \beta\}$ , or  $\{\alpha > 1, \text{ and } \gamma > \beta\}$ . The Jacobian eigenvalues at  $E_3$  in Eq.(9) is

$$\begin{cases} \omega_0 = \frac{1}{2\alpha\gamma-2\beta} \left( \Xi_0 + \frac{\alpha\gamma-\beta}{|\alpha\gamma-\beta|} \Xi_1 \right) & (18a) \\ \omega_1 = \frac{1}{2\alpha\gamma-2\beta} \left( \Xi_0 - \frac{\alpha\gamma-\beta}{|\alpha\gamma-\beta|} \Xi_1 \right), & (18b) \end{cases}$$

where

$$\begin{cases} \Xi_0 = 2\alpha\gamma - \beta^2\mu_0 - (2 + (\alpha - \gamma - 1)\mu_0)\beta & (19a) \\ \Xi_1 = \mu_0 \left[ \beta \left( (4\beta\gamma - 4\gamma^2 + \beta)\alpha^2 - (2\beta^2 + 2\beta\gamma - 4\gamma^2 + 2\beta)\alpha + \beta(\beta - \gamma + 1)^2 \right) \right]^{\frac{1}{2}} & (19b) \end{cases}$$

## 2.4 Properties of Eq.(6) (Type 2)

Similar to Eq.(8), the two-dimensional logistic equations in Eq.(6) (Type 2) have the mappings

$$\begin{cases} f(x, y) = \mu_0 x(1 - x) - \mu_1 xy; & (20a) \\ g(x, y) = -\nu_0 y(1 - y) + \nu_1 xy. & (20b) \end{cases}$$

Eq.(20) has Jacobian that is slightly different from Eq.(9)

$$J = \begin{pmatrix} \mu_0(1 - 2x) - \mu_1 y & -\mu_1 x \\ \nu_1 y & \nu_0(-1 + 2y) + \nu_1 x \end{pmatrix}, \quad (21)$$

with eigenvalues  $\omega_0$  and  $\omega_1$  being, respectively,

$$\begin{cases} \omega_0 = -\mu_0 x + \nu_0 y + \frac{1}{2}(x\nu_1 - y\mu_1) + \frac{1}{2}(\mu_0 - \nu_0) + \frac{\omega}{2} & (22a) \\ \omega_1 = -\mu_0 x + \nu_0 y + \frac{1}{2}(x\nu_1 - y\mu_1) + \frac{1}{2}(\mu_0 - \nu_0) - \frac{\omega}{2} & (22b) \end{cases}$$

where  $\omega$  is the same as in Eq.(11). Fixed points for Eq.(6) (Type 2) are

$$\begin{cases} E'_0 = (0, 0) & (23a) \\ E'_1 = \left(0, 1 + \frac{1}{\nu_0}\right) & (23b) \\ E'_2 = \left(1 - \frac{1}{\mu_0}, 0\right) & (23c) \\ E'_3 = \left(\frac{-\mu_0\nu_0 + \mu_1\nu_0 + \mu_1 + \nu_0}{-\mu_0\nu_0 + \mu_1\nu_1}, \frac{-\mu_0\nu_0 + \mu_0\nu_1 - \mu_0 - \nu_1}{-\mu_0\nu_0 + \mu_1\nu_1}\right) & (23d) \end{cases}$$

However, when  $\mu_0\nu_0 = \mu_1\nu_1$ , Eq.(6) (Type 2) has fixed points  $E'_0$ ,  $E'_1$ , and  $E'_2$ .

We may also make use of **Lemma 1** in Sect. 2.2 to examine the topological type of each fixed point in Eq.(6) (Type 2) as in Theorem 2:

**Theorem 2.** *The topological types of fixed points in Eq.(23) are*

1. For  $E'_0 = (0, 0)$ ,

$$\begin{cases} \Omega(1) = -(\mu_0 - 1)(\nu_0 + 1) \\ \Omega(-1) = -(\mu_0 + 1)(\nu_0 - 1) \\ \det(J) = -\mu_0\nu_0 \\ \text{Tr}(J) = \mu_0 - \nu_0. \end{cases}$$

In this case,

- (a) if  $\mu_0 > 1$ , then  $E'_0$  is a source.
- (b) if  $\mu_0 = 1$ , then  $E'_0$  is a non-hyperbole.

2. For  $E'_1 = (0, 1 + \frac{1}{\nu_0})$ ,

$$\left\{ \begin{array}{l} \Omega(1) = \frac{(\nu_0 + 1)((\mu_0 - \mu_1 - 1)\nu_0 - \mu_1)}{\nu_0} \\ \Omega(-1) = \frac{(\nu_0 + 3)((\mu_0 - \mu_1 + 1)\nu_0 - \mu_1)}{\nu_0} \\ \det(\mathbf{J}) = \frac{(\nu_0 + 2)((\mu_0 - \mu_1)\nu_0 - \mu_1)}{\nu_0} \\ \text{Tr}(\mathbf{J}) = \frac{\nu_0^2 + (\mu_0 - \mu_1 + 2)\nu_0 - \mu_1}{\nu_0}. \end{array} \right.$$

Thus,

- (a) if  $\mu_0 > \frac{\mu_1\nu_0 + \mu_1 + \nu_0}{\nu_0}$ , then  $E'_1$  is a source.
- (b) if  $\mu_0 < \frac{\mu_1\nu_0 + \mu_1 + \nu_0}{\nu_0}$ , then  $E'_1$  is a saddle.
- (c) if  $\mu_0 = \frac{\mu_1\nu_0 + \mu_1 + \nu_0}{\nu_0}$ , then  $E'_1$  is a non-hyperbole.

3. For  $E'_2 = (1 - \frac{1}{\mu_0}, 0)$ ,

$$\left\{ \begin{array}{l} \Omega(1) = \frac{(\mu_0 - 1)((\nu_0 - \nu_1 + 1)\mu_0 + \nu_1)}{\mu_0} \\ \Omega(-1) = \frac{(\mu_0 - 3)((\nu_0 - \nu_1 - 1)\mu_0 + \nu_1)}{\mu_0} \\ \det(\mathbf{J}) = \frac{(\mu_0 - 2)((\nu_0 - \nu_1)\mu_0 + \nu_1)}{\mu_0} \\ \text{Tr}(\mathbf{J}) = -\frac{\mu_0^2 + (\nu_0 - \nu_1 - 2)\mu_0 + \nu_1}{\mu_0}. \end{array} \right.$$

Afterward,

- (a) the fixed point is a sink if one of the following holds:
  - i.  $1 < \mu_0 < 2$  and  $\frac{\nu_1\mu_0 - \mu_0 - \nu_1}{\mu_0} < \nu_0 < \frac{\nu_1\mu_0 + \mu_0 - \nu_1}{\mu_0}$
  - ii.  $\mu_0 = 2$  and  $\frac{\nu_1}{2} - 1 < \nu_0 < \frac{\nu_1}{2} + 1$  with  $\nu_1 > 2$
  - iii.  $2 < \mu_0 < 3$  and  $\frac{\nu_1\mu_0 - \mu_0 - \nu_1}{\mu_0} < \nu_0 < \frac{\nu_1\mu_0 + \mu_0 - \nu_1}{\mu_0}$
- (b) the fixed point is a source if  $\mu_0 > 3$  and  $\nu_0 > \frac{\nu_1\mu_0 + \mu_0 - \nu_1}{\mu_0}$
- (c) the fixed point is a saddle if one of the following holds:
  - i.  $1 \leq \mu_0 < 3$  and  $\nu_0 > \frac{\nu_1\mu_0 + \mu_0 - \nu_1}{\mu_0}$
  - ii.  $\mu_0 > 3$  and  $\frac{\nu_1\mu_0 - \mu_0 - \nu_1}{\mu_0} < \nu_0 < \frac{\nu_1\mu_0 + \mu_0 - \nu_1}{\mu_0}$
  - iii.  $1 < \mu_0$  and  $\nu_0 < \frac{\nu_1\mu_0 - \mu_0 - \nu_1}{\mu_0}$
- (d) the fixed point is a non-hyperbole if one of the following holds:
  - i.  $\mu_1 = 1$
  - ii.  $\nu_0 = \frac{\nu_1\mu_0 - \mu_0 - \nu_1}{\mu_0}$
  - iii.  $\nu_0 = \frac{\nu_1\mu_0 + \mu_0 - \nu_1}{\mu_0}$  and  $\mu_0 \neq 1$
  - iv.  $\mu_0 = 3$  and  $\nu_0 \neq \frac{2\nu_1}{3} + 1$  and  $\nu_0 > \frac{2\nu_1}{3} - 1$

4. For  $E'_3 = \left( \frac{-\mu_0\nu_0 + \mu_1\nu_0 + \mu_1 + \nu_0}{-\mu_0\nu_0 + \mu_1\nu_1}, \frac{-\mu_0\nu_0 + \mu_0\nu_1 - \mu_0 - \nu_1}{-\mu_0\nu_0 + \mu_1\nu_1} \right)$ ,

$$\begin{cases} \Omega(1) = -\frac{\mu_0\nu_0(\nu_0 - \nu_1)(\mu_0 - \mu_1)}{\mu_0\nu_0 - \mu_1\nu_1} \\ \Omega(-1) = \frac{-\nu_0(\nu_0 - \nu_1 + 2)\mu_0^2 + \nu_0(\mu_1 + 2)(\nu_0 - \nu_1 + 2)\mu_0 - 4\mu_1\nu_1}{\mu_0\nu_0 - \mu_1\nu_1} \\ \det(J) = \frac{-\nu_0(\nu_0 - \nu_1 + 1)\mu_0^2 + \nu_0(\mu_1 + 1)(\nu_0 - \nu_1 + 1)\mu_0 - \mu_1\nu_1}{\mu_0\nu_0 - \mu_1\nu_1} \\ \text{Tr}(J) = \frac{-\mu_0^2\nu_0 + \nu_0(\nu_0 + \mu_1 - \nu_1 + 2)\mu_0 - 2\mu_1\nu_1}{\mu_0\nu_0 - \mu_1\nu_1}. \end{cases}$$

As before, conditions for a saddle from **Lemma 1-3** and a non-hyperbole are given as follows:

(a) the fixed point is a saddle if one of the following holds:

- i.  $\mu_0 = 1$  and  $\frac{\nu_0}{\nu_1} < \mu_1$
- ii.  $\mu_0 > 1$ ,  $\mu_1 < \frac{\nu_0\mu_0 - 1}{\nu_0 + 1}$ , and  $\nu_1 < \frac{(\nu_1 + 1)\mu_0}{\mu_0 - 1}$
- iii.  $\mu_0 > 1$ ,  $\nu_1 < \frac{(\nu_0 + 1)\mu_0}{\mu_0 - 1}$ , and  $\frac{\mu_0\nu_0}{\nu_1} < \mu_1$
- iv.  $1 < \mu_0$ ,  $\frac{\mu_0\nu_0}{\nu_1} < \mu_1 < \frac{\nu_0(\mu_0 - 1)}{\nu_0 + 1}$ , and  $\frac{(\nu_0 + 1)\mu_0}{\mu_0 - 1} < \nu_1$

(b) the fixed point is a non-hyperbole if one of the following holds for **Lemma 1-2**:

- i.  $\mu_1 = \frac{\nu_0(\mu_0 - 1)}{\nu_0 + 1}$ ,  $\mu_0 > 1$  and  $\nu_1 < \frac{(\nu_0 + 1)\mu_0}{\mu_0 - 1}$
- ii.  $\nu_1 = \frac{(\nu_0 + 1)\mu_0}{\mu_0 - 1}$ ,  $\mu_0 > 1$ , and  $\mu_1 < \frac{\nu_0(\mu_0 - 1)}{\nu_0 + 1}$
- iii.  $\mu_1 = \frac{\nu_0(\mu_0 - 1)}{\nu_0 + 1}$ ,  $\nu_1 = \frac{(\nu_0 + 1)\mu_0}{\mu_0 - 1}$ , and  $\mu_0 > 1$
- iv.  $\nu_1 = \frac{(\nu_0 + 1)\mu_0}{\mu_0 - 1}$ ,  $\mu_0 > 1$ , and  $\mu_1 > \frac{\nu_0(\mu_0 - 1)}{\nu_0 + 1}$
- v.  $\mu_1 = \frac{\nu_0(\mu_0 - 1)}{\nu_0 + 1}$ ,  $\mu_0 > 1$ , and  $\nu_1 > \frac{(\nu_0 + 1)\mu_0}{\mu_0 - 1}$

(c) the fixed point is a non-hyperbole if one of the following holds for **Lemma 1-1(d)**:

- i.  $1 < \mu_0 < 3$ ,  $\mu_1 = \frac{\nu_0(\mu_0^2\nu_0 - \mu_0^2\nu_1 + 3\mu_0^2 - 3\mu_0\nu_0 + 4\mu_0\nu_1 - 9\mu_0 - 3\nu_1)}{\mu_0\nu_0^2 - \nu_1\mu_0\nu_0 + 4\mu_0\nu_0 - \nu_1\mu_0 + \nu_1\nu_0 + 3\mu_0 - 3\nu_1}$ ,  $\nu_0 < 1$ , and  $\frac{\mu_0(\nu_0 + 1)}{\mu_0 - 1} < \nu_1 < \frac{\mu_0(\nu_0 + 3)}{\mu_0 - 1}$
- ii.  $\mu_0 > 3$ ,  $\mu_1 = \frac{\nu_0(\mu_0^2\nu_0 - \mu_0^2\nu_1 + 3\mu_0^2 - 3\mu_0\nu_0 + 4\mu_0\nu_1 - 9\mu_0 - 3\nu_1)}{\mu_0\nu_0^2 - \nu_1\mu_0\nu_0 + 4\mu_0\nu_0 - \nu_1\mu_0 + \nu_1\nu_0 + 3\mu_0 - 3\nu_1}$ ,  $\nu_0 < 1$ , and  $\frac{\mu_0(\nu_0 + 1)}{\mu_0 - 1} < \nu_1 < \frac{\mu_0(\nu_0^2 + 4\nu_0 + 3)}{\mu_0\nu_0 + \mu_0 - \nu_0 + 3}$
- iii.  $\mu_0 > 3$ ,  $\mu_1 = \frac{\nu_0(\mu_0^2\nu_0 - \mu_0^2\nu_1 + 3\mu_0^2 - 3\mu_0\nu_0 + 4\mu_0\nu_1 - 9\mu_0 - 3\nu_1)}{\mu_0\nu_0^2 - \nu_1\mu_0\nu_0 + 4\mu_0\nu_0 - \nu_1\mu_0 + \nu_1\nu_0 + 3\mu_0 - 3\nu_1}$ ,  $\nu_0 < 1$ , and  $\frac{\mu_0(\nu_0 + 3)}{\mu_0 - 1} < \nu_1 < \frac{\mu_0(\nu_0 + 3)}{\mu_0 - 3}$
- iv.  $1 < \mu_0 < 3$ ,  $\mu_1 = \frac{\mu_0^2\nu_1 - 4\mu_0^2 - 4\mu_0\nu_1 + 12\mu_0 + 3\nu_1}{2(\mu_0\nu_1 - 4\mu_0 + \nu_1)}$ ,  $\nu_0 = 1$ , and  $\frac{2\mu_0}{\mu_0 - 1} < \nu_1 < \frac{4\mu_0}{\mu_0 - 1}$
- v.  $\mu_0 > 3$ ,  $\mu_1 = \frac{\mu_0^2\nu_1 - 4\mu_0^2 - 4\mu_0\nu_1 + 12\mu_0 + 3\nu_1}{2(\mu_0\nu_1 - 4\mu_0 + \nu_1)}$ ,  $\nu_0 = 1$ , and  $\frac{2\mu_0}{\mu_0 - 1} < \nu_1 < \frac{4\mu_0}{\mu_0 - 1}$
- vi.  $\mu_0 > 3$ ,  $\mu_1 = \frac{\mu_0^2\nu_1 - 4\mu_0^2 - 4\mu_0\nu_1 + 12\mu_0 + 3\nu_1}{2(\mu_0\nu_1 - 4\mu_0 + \nu_1)}$ ,  $\nu_0 = 1$ , and  $\frac{4\mu_0}{\mu_0 - 1} < \nu_1 < \frac{4\mu_0}{\mu_0 - 3}$
- vii.  $1 < \mu_0 < 3$ ,  $\mu_1 = \frac{\nu_0(\mu_0^2\nu_0 - \mu_0^2\nu_1 + 3\mu_0^2 - 3\mu_0\nu_0 + 4\mu_0\nu_1 - 9\mu_0 - 3\nu_1)}{\mu_0\nu_0^2 - \nu_1\mu_0\nu_0 + 4\mu_0\nu_0 - \nu_1\mu_0 + \nu_1\nu_0 + 3\mu_0 - 3\nu_1}$ ,  $1 < \nu_0 < 3$ , and  $\frac{\mu_0(\nu_0 + 1)}{\mu_0 - 1} < \nu_1 < \frac{\mu_0(\nu_0 + 3)}{\mu_0 - 1}$
- viii.  $\mu_0 > 3$ ,  $\mu_1 = \frac{\nu_0(\mu_0^2\nu_0 - \mu_0^2\nu_1 + 3\mu_0^2 - 3\mu_0\nu_0 + 4\mu_0\nu_1 - 9\mu_0 - 3\nu_1)}{\mu_0\nu_0^2 - \nu_1\mu_0\nu_0 + 4\mu_0\nu_0 - \nu_1\mu_0 + \nu_1\nu_0 + 3\mu_0 - 3\nu_1}$ ,  $1 < \nu_0 < 3$ , and  $\frac{\mu_0(\nu_0 + 1)}{\mu_0 - 1} < \nu_1 < \frac{\mu_0(\nu_0^2 + 4\nu_0 + 3)}{\mu_0\nu_0 + \mu_0 - \nu_0 + 3}$
- ix.  $\mu_0 > 3$ ,  $\mu_1 = \frac{\nu_0(\mu_0^2\nu_0 - \mu_0^2\nu_1 + 3\mu_0^2 - 3\mu_0\nu_0 + 4\mu_0\nu_1 - 9\mu_0 - 3\nu_1)}{\mu_0\nu_0^2 - \nu_1\mu_0\nu_0 + 4\mu_0\nu_0 - \nu_1\mu_0 + \nu_1\nu_0 + 3\mu_0 - 3\nu_1}$ ,  $1 < \nu_0 < 3$ , and  $\frac{\mu_0(\nu_0 + 3)}{\mu_0 - 1} < \nu_1 < \frac{\mu_0(\nu_0 + 3)}{\mu_0 - 3}$
- x.  $3 > \mu_0 > 1$ ,  $\mu_1 = \frac{3(\mu_0^2\nu_1 - 6\mu_0^2 - 4\mu_0\nu_1 + 18\mu_0 + 3\nu_1)}{4\mu_0(\nu_1 - 6)}$ ,  $\nu_0 = 3$ , and  $\frac{4\mu_0}{\mu_0 - 1} < \nu_1 < \frac{6\mu_0}{\mu_0 - 1}$
- xi.  $\mu_0 > 3$ ,  $\mu_1 = \frac{3(\mu_0^2\nu_1 - 6\mu_0^2 - 4\mu_0\nu_1 + 18\mu_0 + 3\nu_1)}{4\mu_0(\nu_1 - 6)}$ ,  $\nu_0 = 3$ , and  $\frac{4\mu_0}{\mu_0 - 1} < \nu_1 < 6$
- xii.  $\mu_0 > 3$ ,  $\mu_1 = \frac{3(\mu_0^2\nu_1 - 6\mu_0^2 - 4\mu_0\nu_1 + 18\mu_0 + 3\nu_1)}{4\mu_0(\nu_1 - 6)}$ ,  $\nu_0 = 3$ , and  $\frac{6\mu_0}{\mu_0 - 1} < \nu_1 < \frac{6\mu_0}{\mu_0 - 3}$

$$\begin{aligned}
xiii. \quad & 1 < \mu_0 < 3, \mu_1 = \frac{\nu_0(\mu_0^2\nu_0 - \mu_0^2\nu_1 + 3\mu_0^2 - 3\mu_0\nu_0 + 4\mu_0\nu_1 - 9\mu_0 - 3\nu_1)}{\mu_0\nu_0^2 - \nu_1\mu_0\nu_0 + 4\mu_0\nu_0 - \nu_1\mu_0 + \nu_1\nu_0 + 3\mu_0 - 3\nu_1}, \nu_0 > 3, \text{ and } \frac{\mu_0(\nu_0+1)}{\mu_0-1} < \nu_1 < \frac{\mu_0(\nu_0+3)}{\mu_0-1} \\
xiv. \quad & 1 < \mu_0 < 3, \mu_1 = \frac{\nu_0(\mu_0^2\nu_0 - \mu_0^2\nu_1 + 3\mu_0^2 - 3\mu_0\nu_0 + 4\mu_0\nu_1 - 9\mu_0 - 3\nu_1)}{\mu_0\nu_0^2 - \nu_1\mu_0\nu_0 + 4\mu_0\nu_0 - \nu_1\mu_0 + \nu_1\nu_0 + 3\mu_0 - 3\nu_1}, \nu_0 > 3, \text{ and } \frac{\mu_0(\nu_0+1)}{\mu_0-1} < \nu_1 < \frac{\mu_0(\nu_0^2+4\nu_0+3)}{\mu_0\nu_0+\mu_0-\nu_0+3} \\
xv. \quad & \mu_0 > 3, \mu_1 = \frac{\nu_0(\mu_0^2\nu_0 - \mu_0^2\nu_1 + 3\mu_0^2 - 3\mu_0\nu_0 + 4\mu_0\nu_1 - 9\mu_0 - 3\nu_1)}{\mu_0\nu_0^2 - \nu_1\mu_0\nu_0 + 4\mu_0\nu_0 - \nu_1\mu_0 + \nu_1\nu_0 + 3\mu_0 - 3\nu_1}, \nu_0 > 3, \text{ and } \frac{\mu_0(\nu_0+3)}{\mu_0-1} < \nu_1 < \frac{\mu_0(\nu_0+3)}{\mu_0-3}
\end{aligned}$$

Also by Hypothesis H<sub>2</sub>, in terms of  $\alpha$ ,  $\beta$ , and  $\gamma$ ,  $E'_3$  in Eq.(23d) is  $E'_3 = \left( \frac{\alpha\beta\mu_0 - \beta\mu_0 + \alpha + \beta}{\mu_0(\alpha\gamma - \beta)}, \frac{-\beta\mu_0 + \gamma\mu_0 - \gamma - 1}{\mu_0(\alpha\gamma - \beta)} \right)$ .  
Jacobian eigenvalues of  $E'_3$  in Eq.(21) is

$$\begin{cases} \omega_0 = \frac{1}{2\alpha\gamma - 2\beta} \left( \Xi'_0 + \frac{\alpha\gamma - \beta}{|\alpha\gamma - \beta|} \Xi'_1 \right) & (28a) \\ \omega_1 = \frac{1}{2\alpha\gamma - 2\beta} \left( \Xi'_0 - \frac{\alpha\gamma - \beta}{|\alpha\gamma - \beta|} \Xi'_1 \right), & (28b) \end{cases}$$

where

$$\begin{cases} \Xi'_0 = (2\gamma - 1)\alpha - \beta^2\mu_0 - (\alpha\mu_0 + (-\mu_0 + 1)\gamma - \mu_0 + 4)\beta & (29a) \\ \Xi'_1 = \left( (\mu_0 - 1) \left( (-4\beta\mu_0 - 4)\alpha^2 + 4\beta(\mu_0 - 1)\alpha + \beta^2(\mu_0 - 1) \right) \gamma^2 \right. & (29b) \\ \quad \left. + \left( 4(\beta\mu_0 + 1)^2\alpha^2 - 2\beta(\mu_0 - 1)(\beta\mu_0 + 1)\alpha - 2\beta^2\mu_0(\mu_0 - 1)(\beta + 1) \right) \gamma \right. & \\ \quad \left. + \left( (\beta\mu_0 + 1)\alpha - \beta\mu_0(\beta + 1) \right)^2 \right)^{\frac{1}{2}} & (29c) \end{cases}$$

Eq.(28) shows that whenever  $\Xi'_1$  is negative,  $\omega_0$  and  $\omega_1$  are complex conjugates. Unlike the previous case, the fixed points  $E'_1$ ,  $E'_2$ , and  $E'_3$  now depend on the growth rate  $\mu_0$ .

## 2.5 Corresponding relationships between Eq.(5) (Type 1) and Eq.(6) (Type 2)

In this subsection we would like to demonstrate that, after linear transformation, Eq.(5) (Type 1) is similar to Eq.(6) (Type 2). The only difference is that we need to find appropriate parameters for different sets of equations. First, rewrite Eq.(8) as

$$\begin{cases} \bar{f}(x, y) = \mu'_0x - \mu'_0x^2 - \mu'_1xy + x = \mu'_0x(1 - x) - \mu'_1xy + x; & (30a) \\ \bar{g}(x, y) = -\nu'_0y + \nu'_0y^2 - \nu'_1xy + y = -\nu'_0y(1 - y) + \nu'_1xy + y. & (30b) \end{cases}$$

Also Eq.(20) is written as

$$\begin{cases} f(X, Y) = \mu_0X - \mu_0X^2 - \mu_1XY = \mu_0X(1 - X) - \mu_1XY; & (31a) \\ g(X, Y) = -\nu_0Y + \nu_0Y^2 + \nu_1XY = -\nu_0Y(1 - Y) + \nu_1XY. & (31b) \end{cases}$$

We consider the linear transformation as follows

$$\begin{cases} x = \alpha_X X + \alpha_Y Y + \alpha_0; & (32a) \\ y = \beta_X X + \beta_Y Y + \beta_0, & (32b) \end{cases}$$

where  $\alpha_X$ ,  $\alpha_Y$ ,  $\alpha_0$ ,  $\beta_X$ ,  $\beta_Y$ , and  $\beta_0$  are about to be determined with comparisons. Substituting into Eq.(30), we obtain

$$\begin{aligned}
\bar{f}(X, Y) &= \mu'_0(\alpha_X X + \alpha_Y Y + \alpha_0) - \mu'_0(\alpha_X X + \alpha_Y Y + \alpha_0)^2 \\
&\quad - \mu'_1(\alpha_X X + \alpha_Y Y + \alpha_0)(\beta_X X + \beta_Y Y + \beta_0) + (\alpha_X X + \alpha_Y Y + \alpha_0) \\
&= \mu'_0 \alpha_X X + \mu'_0 \alpha_Y Y + \mu'_0 \alpha_0 \\
&\quad - \mu'_0(\alpha_X^2 X^2 + \alpha_Y^2 Y^2 + \alpha_0^2 + 2\alpha_X \alpha_Y XY + 2\alpha_0 \alpha_X X + 2\alpha_0 \alpha_Y Y) \\
&\quad - \mu'_1[\alpha_X \beta_X X^2 + \alpha_Y \beta_Y Y^2 + \alpha_0 \beta_0 \\
&\quad\quad + (\alpha_X \beta_Y + \alpha_Y \beta_X)XY + (\alpha_X \beta_0 + \alpha_0 \beta_X)X + (\alpha_Y \beta_0 + \beta_Y \alpha_0)Y] \\
&\quad + (\alpha_X X + \beta_Y Y + \alpha_0) \\
&= [\mu'_0 \alpha_X - \mu'_0 \cdot 2\alpha_0 \alpha_X - \mu'_1 \cdot (\alpha_X \beta_0 + \alpha_0 \beta_X) + \alpha_X] X & (33a) \\
&\quad - (\mu'_0 \alpha_X^2 + \mu'_1 \alpha_X \beta_X) X^2 & (33b) \\
&\quad + (-\mu'_0 \cdot 2\alpha_X \alpha_Y - \mu'_1(\alpha_X \beta_Y + \alpha_Y \beta_X)) XY & (33c) \\
&\quad - (-\mu'_0 \alpha_Y + \mu'_0 \cdot 2\alpha_0 \alpha_Y + \mu'_1(\alpha_Y \beta_0 + \alpha_0 \beta_Y) - \beta_Y) Y & (33d) \\
&\quad + (-\mu'_0 \alpha_Y^2 + \mu'_1 \alpha_Y \beta_Y) Y^2 & (33e) \\
&\quad + (\mu'_0 \alpha_0 - \mu'_1 \alpha_0 \beta_0 - \mu'_0 \alpha_0^2 + \alpha_0) & (33f)
\end{aligned}$$

Similarly,

$$\begin{aligned}
\bar{g}(X, Y) &= -\nu'_0(\beta_X X + \beta_Y Y + \beta_0) + \nu'_0(\beta_X X + \beta_Y Y + \beta_0)^2 \\
&\quad + \nu'_1(\alpha_X X + \alpha_Y Y + \alpha_0)(\beta_X X + \beta_Y Y + \beta_0) + (\beta_X X + \beta_Y Y + \beta_0) \\
&= -\nu'_0 \beta_X X - \nu'_0 \beta_Y Y - \nu'_0 \beta_0 \\
&\quad + \nu'_0(\beta_X^2 X^2 + \beta_Y^2 Y^2 + \beta_0^2 + 2\beta_X \beta_Y XY + 2\beta_0 \beta_X X + 2\beta_0 \beta_Y Y) \\
&\quad + \nu'_1[\alpha_X \beta_X X^2 + \alpha_Y \beta_Y Y^2 + \alpha_0 \beta_0 \\
&\quad\quad + (\alpha_X \beta_Y + \alpha_Y \beta_X)XY + (\alpha_X \beta_0 + \alpha_0 \beta_X)X + (\alpha_Y \beta_0 + \alpha_0 \beta_Y)Y] \\
&\quad + (\beta_X X + \beta_Y Y + \beta_0) \\
&= [-\nu'_0 \beta_X + \nu'_0 \cdot 2\beta_0 \beta_X + \nu'_1(\alpha_X \beta_0 + \alpha_0 \beta_X) + \beta_X] X & (34a) \\
&\quad - (-\nu'_0 \beta_X^2 - \nu'_1 \alpha_X \beta_X) X^2 & (34b) \\
&\quad - (-\nu'_0 \cdot 2\beta_X \beta_Y - \nu'_1(\alpha_X \beta_Y + \alpha_Y \beta_X)) XY & (34c) \\
&\quad - (+\nu'_0 \beta_Y - \nu'_0 \cdot 2\beta_0 \beta_Y - \nu'_1(\alpha_Y \beta_0 + \alpha_0 \beta_Y) - \beta_Y) Y & (34d) \\
&\quad + (+\nu'_0 \beta_Y^2 + \nu'_1 \alpha_Y \beta_Y) Y^2 & (34e) \\
&\quad + (-\nu'_0 \beta_0 + \nu'_0 \beta_0^2 + \nu'_1 \alpha_0 \beta_0 + \beta_0) & (34f)
\end{aligned}$$

Transformation from Eq.(30) to Eq.(31) may be accomplished if we choose coefficients in Eq.(33a), Eq.(33b), Eq.(33f), Eq.(34d), Eq.(34e), and Eq.(34f) to be all zero, coefficient in Eq.(33c) equal to  $\nu_1$ , coefficients in Eq.(33d) and Eq.(33e) both equal to  $\nu_0$ , coefficients in Eq.(34a) and Eq.(34b) both equal to  $\mu_0$ , and coefficient in Eq.(34c) equal to  $\mu_1$ . Subsequently,

$$\begin{cases} \bar{f}(X, Y) = -\nu_0 Y + \nu_0 Y^2 + \nu_1 XY = g(X, Y), & (35a) \\ \bar{g}(X, Y) = \mu_0 X - \mu_0 X^2 - \mu_1 XY = f(X, Y). & (35b) \end{cases}$$



Non-trivial solutions for coefficients in Eq.(32) are,

$$\alpha_X = \frac{(-\nu_0\mu_0 + \nu_1\mu_0 + \mu_0 + \nu_1)\mu_1}{(-\nu_0\mu_0 + \nu_1\mu_1)\mu_0} \quad (36a)$$

$$\alpha_Y = \frac{\nu_0\mu_0 - \mu_1\nu_0 + \mu_1 + 2\nu_0 + \nu_1}{-\nu_0\mu_0 + \nu_1\mu_1} \quad (36b)$$

$$\beta_X = \frac{\nu_0\mu_0 - \nu_1\mu_0 - \mu_0 - \nu_1}{-\nu_0\mu_0 + \nu_1\mu_1} \quad (36c)$$

$$\beta_Y = \frac{-\nu_1(\nu_0\mu_0 - \mu_1\nu_0 + \mu_1 + 2\nu_0 + \nu_1)}{(-\nu_0\mu_0 + \nu_1\mu_1)\nu_0} \quad (36d)$$

$$\alpha_0 = \frac{-\nu_0\mu_0 + \mu_1\nu_0 - \mu_1 - \nu_0}{-\nu_0\mu_0 + \nu_1\mu_1} \quad (36e)$$

$$\beta_0 = \frac{-\nu_0\mu_0 + \nu_1\mu_0 + \mu_0 + \nu_1}{-\nu_0\mu_0 + \nu_1\mu_1}, \quad (36f)$$

which give us the relationships of parameters between Eq.(30) and Eq.(31) as follows

$$\left\{ \begin{array}{l} -\frac{(\mu'_0(\nu'_0 - \nu'_1 - 1) - \nu'_1)^2}{\mu'_0(\mu'_0\nu'_0 - \mu'_1\nu'_1)} = \mu_0 \end{array} \right. \quad (37a)$$

$$\left\{ \begin{array}{l} -\frac{(\nu'_0(\mu'_0 - \mu'_1 + 2) + \mu'_1 + \nu'_1)^2}{\nu'_0(\mu'_0\nu'_0 - \mu'_1\nu'_1)} = \nu_0 = \beta\mu_0 \end{array} \right. \quad (37b)$$

$$\left\{ \begin{array}{l} \frac{\nu'_1((\nu'_0 - \nu'_1 - 1)\mu'_0 - \nu'_1)(\mu'_0\nu'_0 + \nu'_0(2 - \mu'_1) + \mu'_1 + \nu'_1)}{\mu'_0\nu'_0(\mu'_0\nu'_0 - \mu'_1\nu'_1)} = \mu_1 = \alpha\mu_0 \end{array} \right. \quad (37c)$$

$$\left\{ \begin{array}{l} \frac{\mu'_1((\nu'_0 - \nu'_1 - 1)\mu'_0 - \nu'_1)(\mu'_0\nu'_0 + \nu'_0(2 - \mu'_1) + \mu'_1 + \nu'_1)}{\mu'_0\nu'_0(\mu'_0\nu'_0 - \mu'_1\nu'_1)} = \nu_1 = \gamma\mu_0 \end{array} \right. \quad (37d)$$

Interestingly, we note that  $\frac{\mu'_1\nu'_1}{\mu'_0\nu'_0} = \frac{\mu_1\nu_1}{\mu_0\nu_0}$  and  $\mu_1\mu'_1 = \nu_1\nu'_1$ . Unfortunately, general solutions of  $\mu'_0$ ,  $\mu'_1$ ,  $\nu'_0$ , and  $\nu'_1$  in terms of  $\mu_0$ ,  $\mu_1$ ,  $\nu_0$ , and  $\nu_1$  are difficult to find. However, if we notice that since

$$\left\{ \begin{array}{l} \nu_1^2 = \frac{\mu_1^2}{\mu_0\nu_0} \mu'_0\nu'_0; \end{array} \right. \quad (38a)$$

$$\left\{ \begin{array}{l} \mu_1^2 = \frac{\nu_1^2}{\mu_0\nu_0} \mu'_0\nu'_0, \end{array} \right. \quad (38b)$$

we then further acquire parameters of the system in Eq.(30), in the counterpart of that in Eq.(31),

$$\left\{ \begin{array}{l} \alpha' \equiv \frac{\mu'_1}{\mu'_0} = \frac{\nu_1}{\sqrt{\mu_0\nu_0}} \sqrt{\frac{\nu'_0}{\mu'_0}} = \frac{\gamma\mu_0\sqrt{\beta'}}{\sqrt{\mu_0\beta\mu_0}} = \frac{\gamma}{\sqrt{\beta}} \sqrt{\beta'}; \end{array} \right. \quad (39a)$$

$$\left\{ \begin{array}{l} \beta' \equiv \frac{\nu'_0}{\mu'_0} \end{array} \right. \quad (39b)$$

$$\left\{ \begin{array}{l} \gamma' \equiv \frac{\nu'_1}{\mu'_0} = \frac{\mu_1}{\sqrt{\mu_0\nu_0}} \sqrt{\frac{\nu'_0}{\mu'_0}} = \frac{\alpha\mu_0\sqrt{\beta'}}{\sqrt{\mu_0\beta\mu_0}} = \frac{\alpha}{\sqrt{\beta}} \sqrt{\beta'}, \end{array} \right. \quad (39c)$$

Therefore, once  $\alpha$ ,  $\beta$ , and  $\gamma$  in the system described in Eq.(31) (Eq.(20)) in Sect. 2.4 are determined, we should be able to reconstruct a similar bifurcation diagram in the system in Eq.(30) (Eq.(8)) in Sect. 2.3 with the parameters  $\alpha'$ ,  $\beta'$ , and  $\gamma'$ . Therefore, in this study, we show only bifurcation diagrams for Eq.(6) (Type 2).

## 2.6 Lyapunov exponents

In addition, the chaotic behavior may be better examined by introducing Lyapunov exponents, which are defined as, base 2 being chosen to conform to Wolf et al.[36],

$$\left\{ \begin{array}{l} \lambda_x \equiv \log_2 |w_0| = \frac{\ln |w_0|}{\ln 2} \\ \lambda_y \equiv \log_2 |w_1| = \frac{\ln |w_1|}{\ln 2}. \end{array} \right. \quad (40a)$$

$$\quad (40b)$$

The positive value of  $\lambda_x$  or  $\lambda_y$ , together with the negative value of the total sum of the Lyapunov exponent, either  $\sum \lambda_x < 0$  or  $\sum \lambda_y < 0$ , are strong inferences of chaos for the prey or predator[37]. For comparison, Lyapunov exponents of time series data of prey and predator populations were also calculated by both the algorithms of Rosenstein[29] and Eckmann et al.[30] with the package of NOnLinear measures for Dynamical Systems (nolds)[38]. For the Rosenstein algorithm, the embedding dimension for delay embedding was `emb.dim = 10`, and the step size between time series data points was set at  $\tau = 1$  seconds. While the number of data points (`trajectory_len`) was set to 20 and used for the distance trajectories between two neighboring points, the mean period of the time series data, obtained from the fast Fourier transform, was used as the minimal temporal separation (`min_tsep`) between two neighbors. The search for the appropriate delay was terminated when several potential neighbors of a vector were found to be smaller than the minimal neighbors, which were set as `min_neighbors = 20`. Finally, the RANSAC fitting was used for the line fitting. For the algorithm proposed by Eckmann et al., the matrix dimension was set to 2, and the embedding dimension was set to 10 as in the Rosenstein algorithm. Furthermore,  $\tau = 1$  s, the minimum number of neighbors (`min_nb`) was 4, and `min_tsep = 0` were used in the algorithm.

There are at least four disadvantages for the above algorithms, as mentioned by Escot and Galan[37]: lack of the ability to estimate the full Lyapunov spectrum, not resilient to noise in time-series data, poor detection performance in nonlinearity with an adequate sample size, and no theoretical derivations for the algorithms about their consistency and asymptotic distributions, making it impossible to statistically infer with respect to chaos.

## 3 Results and Discussions

In the present study, we focus only on drawings of the equations in Sect. 2.4. We observed that there could be four different bifurcation diagrams with various kinds of combinations of parameters. The first category is **Normal**, referring to normal competitive behavior in the increasing and decreasing number of species between the prey and the predator. The second category is **Standard**, referring to the standard bifurcation diagram as shown in the well-known 1D logistic equation in the prey in the absence of the predator. The third category is **Extinction**, where a small value  $\beta$  plays an important role in contributing to this phenomenon, which is different from previous study[28], connoting to extinction of the predator when the prey becomes chaotic. The fourth category is named **Vorticella** because its topological shape resembles the vorticella. The categories and parameters are summarized in Table 1. `initX` and `initY` indicate the initial values of the prey and the predator, respectively. Special attention should be paid to the cases of Normal and Extinction, where the inters-pecies parameters are deliberately made the same, but the initial population was different: for Normal, the two species have the same initial population, whereas for Extinction, the predator has 10 times more population than the prey. The discrepancy in the initial population in these two cases shows completely different evolution consequences. Furthermore, to minimize variations between parameters, `initX`, `initY`,  $\alpha$ , and  $\beta$  are chosen to be the same for **Standard**, **Vorticella**, and **Extinction** to demonstrate the topological dependence on  $\gamma$ . Detailed discussions of the topology dependence on  $\gamma$  are given in Sect. 3.1.

Regarding the Lyapunov exponents, Equation, Rosenstein, Eckmann X, and Eckmann Y in the legend of  $\lambda_x$  and  $\lambda_y$  refer to calculations directly from Eq.(40), from the time-series algorithm of Rosenstein, Eckmann et al. of the prey, and Eckmann et al. of the predator, respectively. Comparisons of sum of Lyapunov exponents for every algorithm are summarized in Table 2. The codes, together with animations on population iterations, phase portraits, and phase diagrams under different growth rates, can be retrieved via Ref([39]).

	initX	initY	$\alpha$	$\beta$	$\gamma$
Normal	0.200	0.200	1.000	0.001	0.500
Standard <sup>1</sup>	0.010	0.100	1.000	0.001	0.197
Extinction	0.010	0.100	1.000	0.001	0.500
Vorticella	0.010	0.100	1.000	0.001	0.912

Table 1: Parameters used for simulations used in Sect. 2.4.

<sup>1</sup>Parameters of 0.100, 0.500, 1.000, 0.100, 0.500 also produce Standard, which made a perfect 0, in the sense of computer error, for  $y$ . These parameters were used to make both Rosenstein and Eckmann et al. algorithms work. The small value  $\beta$  also makes contributions to the first term in Eq.(6b), and it can be confirmed by examining its order of magnitudes.

$\sum \lambda$	Eq.(40a) $\lambda_x$	Eq.(40b) $\lambda_y$	Rosenstein $\lambda_x$	Rosenstein $\lambda_y$	Eckmann et al. $\lambda_x$	Eckmann et al. $\lambda_y$
Normal	-357.012	-365.094	-76.198	-162.843	-148.710	-262.202
Standard	-321.133	-698.992	-115.988	-443.234	Not reliable	Not reliable
Extinction	-326.102	-336.777	-103.789	-204.999	-135.607	-269.497
Vorticella	-332.520	-201.130	-58.598	-125.890	-59.522	-142.697

Table 2: Comparison of sum of Lyapunov for every algorithm with same parameters in Table 1.

### 3.1 $\gamma$ dependence of the topological transformation in the bifurcation diagram

Before discussing about each bifurcation diagram, first we show the topological variations of bifurcation diagram depending on  $\gamma$  when all the other parameters are kept the same for **Standard**, **Extinction**, and **Vorticella** given in Table 1. In Figure 1, simulations show that as  $\gamma < 0.431$ , the bifurcation diagram is classified as **Standard** with negligible  $y$ . The detained discussions on **Standard** are given in Sect. 3.3. However, significant  $y$  begins to appear around  $\mu_0 = 3.7$  after  $\gamma = 0.445$ , *breaking* the structure of **Standard** for  $x$ , as shown in Figure 1a, while gradually transforming the topology into **Extinction**. When  $0.480 < \gamma < 0.666$ , the bifurcation diagram falls into the topology of **Extinction**, as in Figure 1b. More detailed discussions on **Extinction** are given in Sect. 3.4. Meanwhile, the predictable values  $x$  and  $y$  as in **Normal** appear within  $3.5 < \mu_0 < 3.7$  (see Figure 1b). Subsequently, **Vorticella** grows out of the disappearance of **Extinction**, see Figure 1c. After  $\gamma > 0.694$ , the bifurcation diagram becomes **Vorticella**, as shown in Figure 1d. The detained discussions on **Vorticella** are also given in Sect. 3.5. In the range  $0.431 < \gamma < 0.480$ , both **Standard** and **Extinction** coexist (see Figure 1a). On the other hand, in the range  $0.666 < \gamma < 0.694$ , the bifurcation diagram is considered as **Normal**, regardless of some small black regions around  $\mu_0 = 2.5$  and  $\mu_0 = 4.0$ , the latter exhibits chaos that may be confirmed by the Lyapunov exponents shown below. Within the range, **Extinction** and **Vorticella** appear simultaneously (see Figure 1c). Another pure **Normal** bifurcation without any chaos region is given in Sect. 3.2.

It is much more interesting to plot bifurcation diagrams in three dimensions, as shown in Figure 2 with an elevation angle  $20^\circ$  and an azimuthal angle  $60^\circ$ . Figure 1a shows the case with  $\gamma = 0.455$ , where stable orbitals originally lying in  $x - \mu_0$  within the range  $3.6 < \mu_0 < 3.8$  now become blurred and instead grow in the  $x - y$  plane, forming a structure similar to **Standard** within the range  $3.0 < \mu_0 < 3.6$ . Figure 2b with  $\gamma = 0.480$  shows a butterfly structure of **Extinction** as in Figure 10. Figure 2c shows the 3D bifurcation diagram of **Normal** with  $\gamma = 0.666$ . In addition to normal competing behavior in the middle, there is a blacked-in area at the top and a spiral-in attractor at the bottom of the  $y - \mu_0$  plane. Meanwhile, a stripe appears around  $\mu_0 \approx 4.0$ , showing the last occurrence of **Extinction**. Figure 2d shows the three-dimensional bifurcation diagram at the beginning of **Viracella** with  $\gamma = 0.694$ , with the chaotic blacked region shown at the bottom.

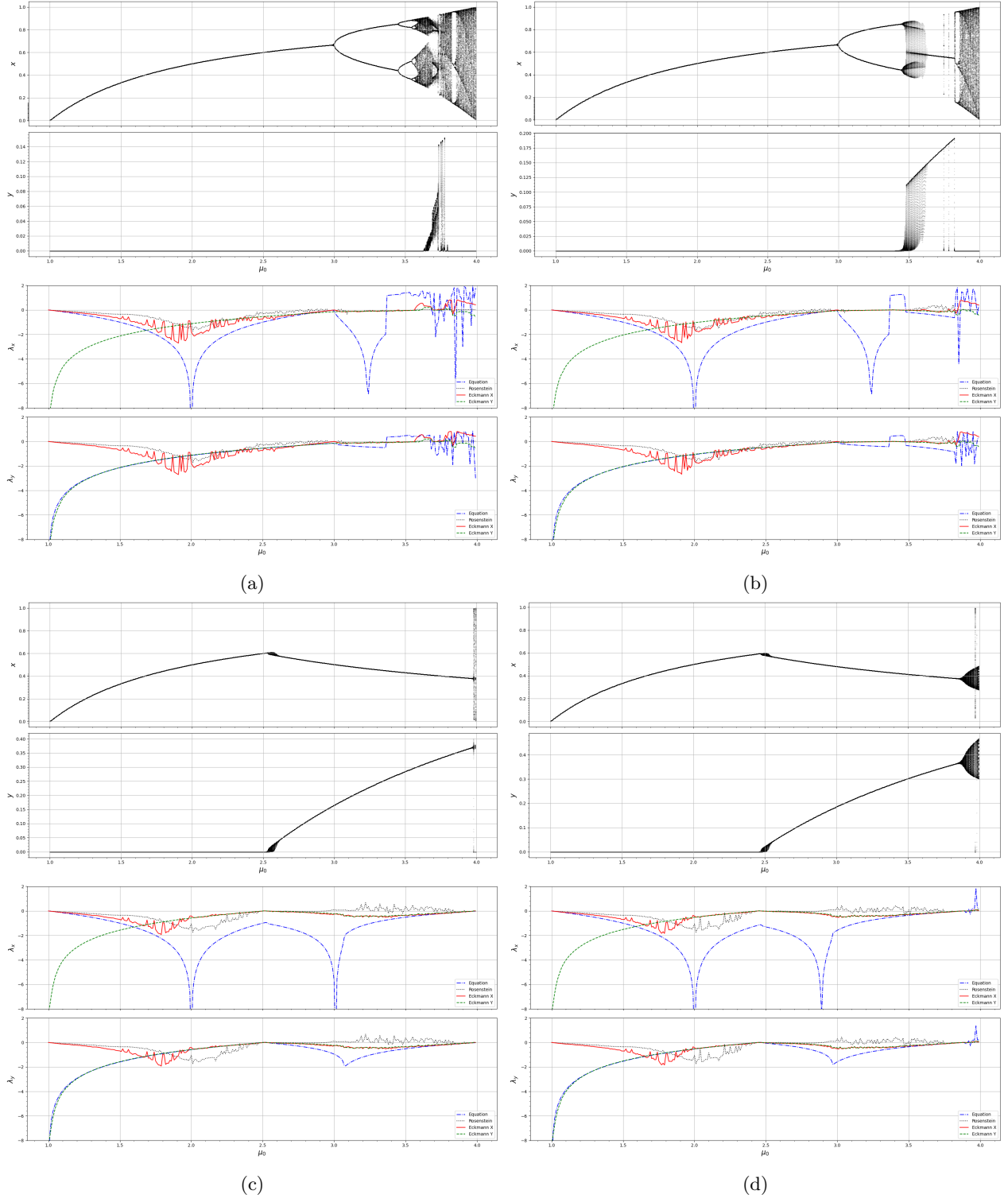


Figure 1: Topological Dependence on  $\gamma$  of bifurcation diagrams, together with corresponding Lyapunov exponents calculated from Eq.(40), are compared.  $\gamma$  for (1a), (1b), (1c) and (1d) are 0.455, 0.480, 0.666, and 0.694, respectively.

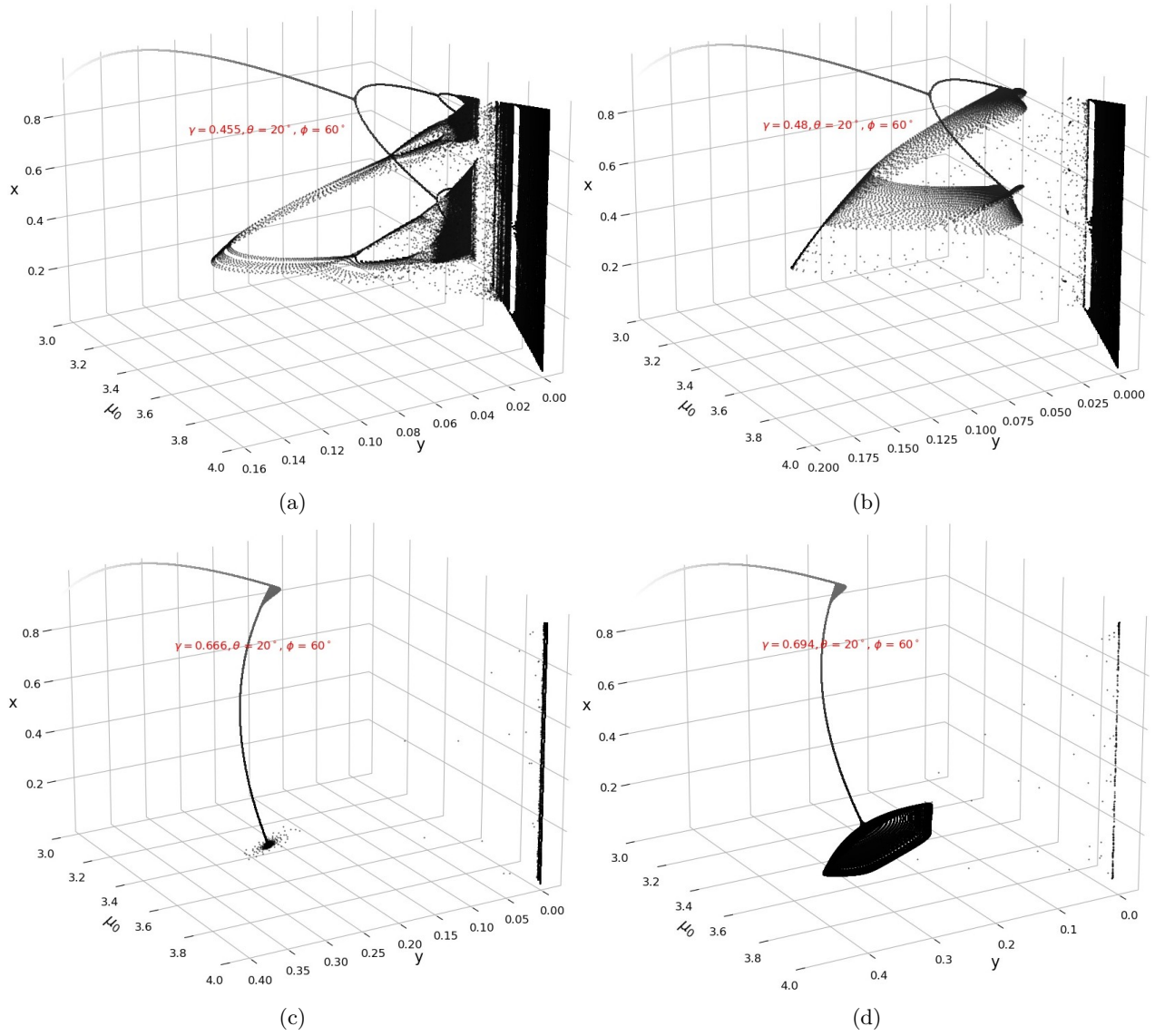
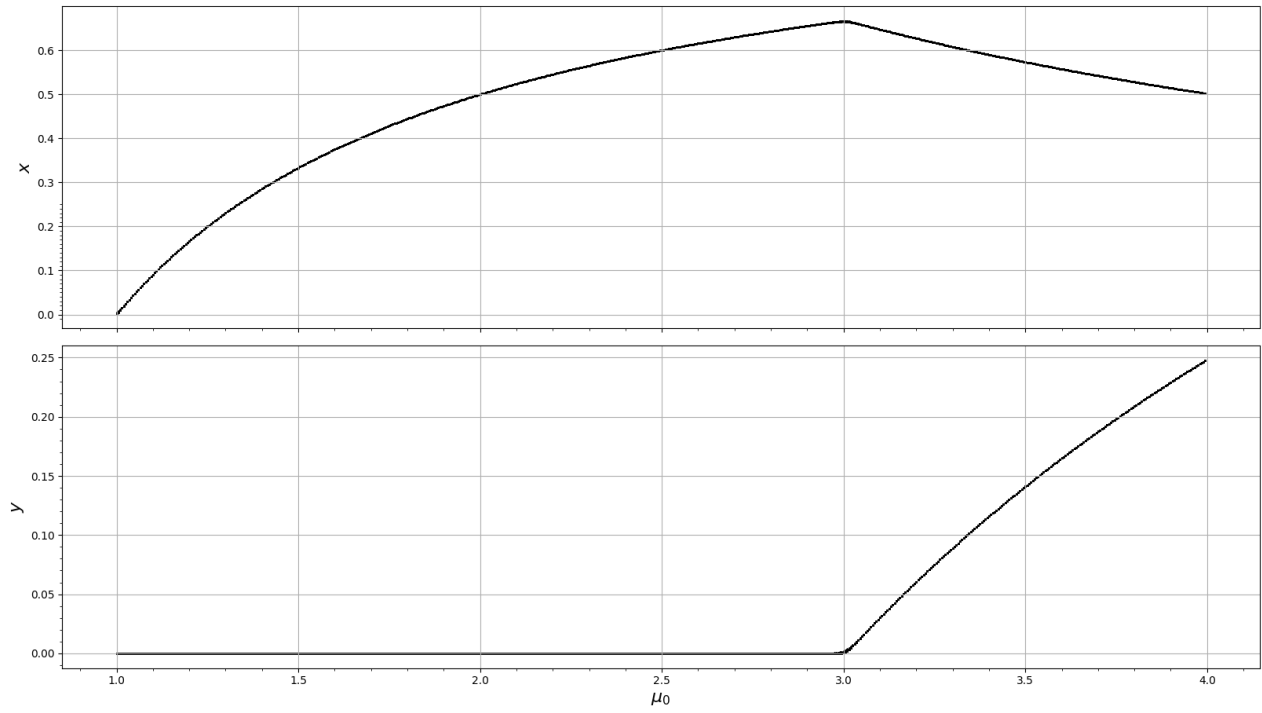


Figure 2: 3D phase portrait for various  $\gamma$  values viewed at an elevation angle  $20^\circ$  and an azimuthal angle  $60^\circ$

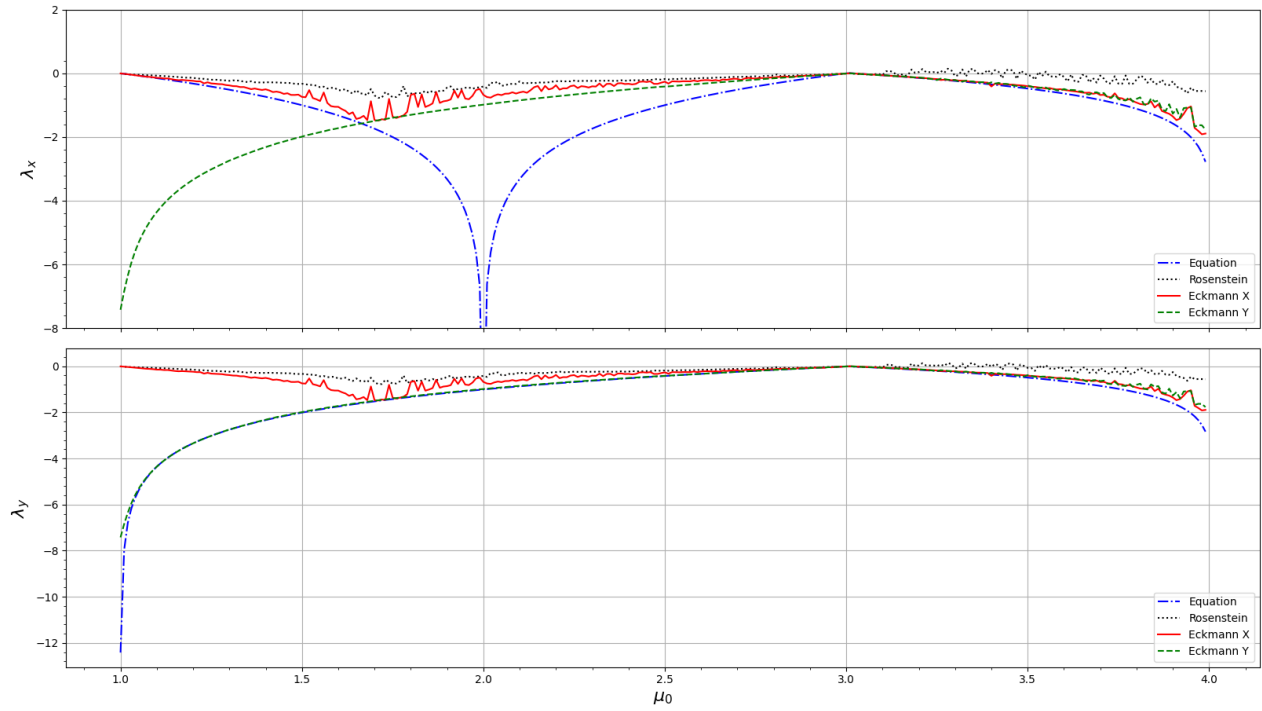
## 3.2 Normal

Our dynamical system may describe normal competitiveness without chaos, compared with Figure 1c showing slight chaos regins at  $\mu_0$  around 2.5 and 4.0, between two species. Under the circumstance of an equal initial population, Figure 3a shows a steadily increasing population of  $x$  in the absence of predator when  $\mu_0 < 3.0$ . At the appearance of  $y$  after  $\mu_0 > 3.0$ , the prey gradually decreases with the number of predators.

Figure 3b ensures that in this scenario there is no chaos, as the Lyapunou exponents calculated by every algorithm are negative. However, the results are different from those of various algorithms. First, for  $\lambda_x$ , there is a trench around  $\mu_0 = 2$  by Eq.(40), whereas all other algorithms fail to reproduce. Rosenstein, Eckmann X, and Eckmann Y only reproduced a shallow dip around  $1.5 < \mu_0 < 2.5$ . Furthermore, we observe that Rosenstein and Eckmann X have quite similar results in the entire range of  $\mu_0$ , except that Rosenstein has a slightly higher value. Furthermore, Eckmann X and Eckmann Y have almost identical values when  $\mu_0 > 1.66$ , but Eckmann Y digresses a lot from the other three curves with a low growth rate below  $\mu_0 = 1.66$ . For  $\lambda_y$ , all algorithms show a close spectrum  $\mu_0 > 1.692$ , with larger values for Rosenstein. The four algorithms divide into two groups of results below  $\mu_0 = 1.692$ , with Rosenstein and Eckmann X showing an increasing tail that is different from the other two algorithms showing curves of drop.



(a)



(b)

Figure 3: Competitive behavior and Lyapunov exponents of Normal.

### 3.3 Standard

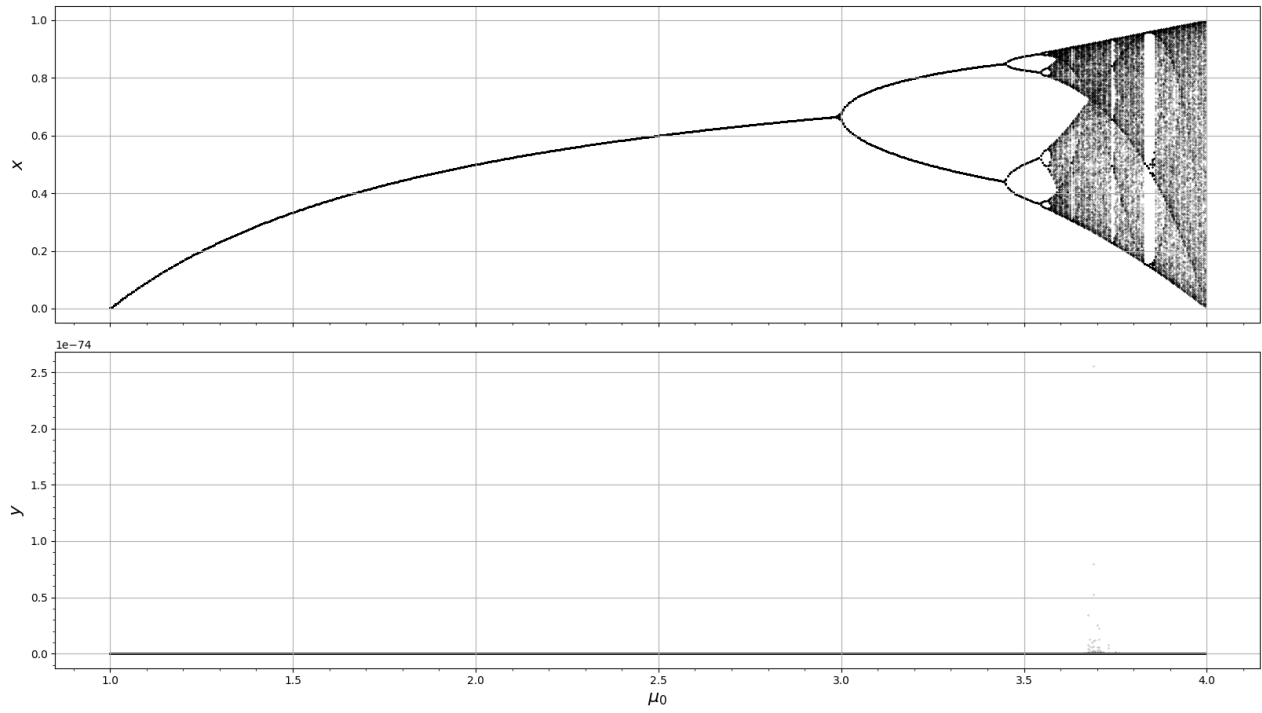
Figure 4a shows the bifurcation diagram and the Lyapunov exponents of Standard. Our model shows that even with nonzero initial population and nonzero inter-species relationships of  $\alpha$ ,  $\beta$ , and  $\gamma$ , we may still acquire a flip bifurcation for 1D logistic equation[40] for the prey in the absence of the predator. A flip bifurcation is a counterpart in the discrete dynamical system to describe the concept of periodic doubling in the continuous dynamic system[41].

Figure 4b shows the Lyapunov exponents. We may see that for the general trend, all algorithms show that both  $\lambda_x$  and  $\lambda_y$  are negative for  $\mu_0 < 3.0$ , while  $\lambda_x$  and  $\lambda_y$  have positive and negative values for  $\mu_0 > 3.5$ . It is widely accepted[42] that the Lyapunov exponent values occur interchangeably between positive and negative inferring chaos, which is consistent with the shaded area in Figure 4a. Another inconsistency occurs with  $3.0 < \mu_0 < 3.5$  with  $\lambda_x > 0$  for Eq.(40) but  $\lambda_x < 0$  for all other algorithms, where  $x$  exhibits a flip bifurcation from 2-cycle into 4-cycle. Nevertheless, this inconsistency may not be a problem for us to distinguish chaos from happening. There is a break around  $\mu_0 = 2$  for Eckmann X in both  $\lambda_x$  and  $\lambda_y$ , at which Eq.(40) shows a deep trench in  $\lambda_x$ .

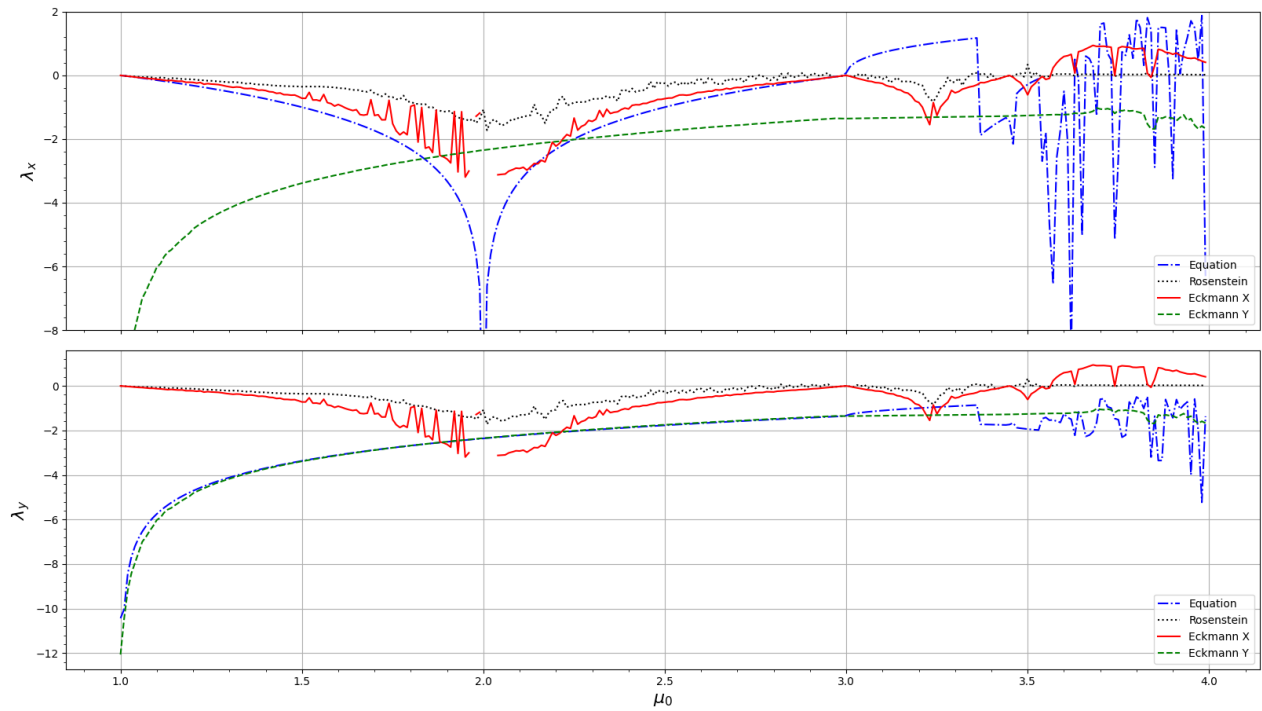
Figure 5 studies the population in the course of time (iteration) at  $\mu_0$  equal to 2.700 (1-cycle), 3.000 (2-cycle where the flip bifurcation occurs) and 3.500 (4-cycle), 3.700 (at which the system goes into chaos), 3.840 (the system returning to a more stable 3-cycle) and 3.945 (where the system returns to chaos again) in successive order. The zero predator population is obtained over the course of time.

Figure 6 shows the absolute values of the eigenvalues  $\omega_0$  and  $\omega_1$  at fixed points  $E'_1$ ,  $E'_2$  and  $E'_3$ . The topological types of fixed points may be checked more straightforwardly with the figure. The first and third columns show that  $E'_1$  and  $E'_3$  are sources because  $\omega_0$  and  $\omega_1$  are always greater than 1. The second column shows that  $E'_2$  is a sink when  $1 < \mu_0 < 3$  and at  $3 < \mu_0 < 4$ ,  $E'_2$  is a saddle. Non-hyperboles can also be examined at  $\mu_0 = 1$  and  $\mu_0 = 3$  for  $E'_2$  (in both cases  $\omega_0 = 1$  and  $\omega_1 \neq 1$ ). Finally, when  $\mu_0 > 3$ ,  $E'_2$  is a source.





(a)



(b)

Figure 4: Bifurcation diagram and Lyapunov exponents of Standard.

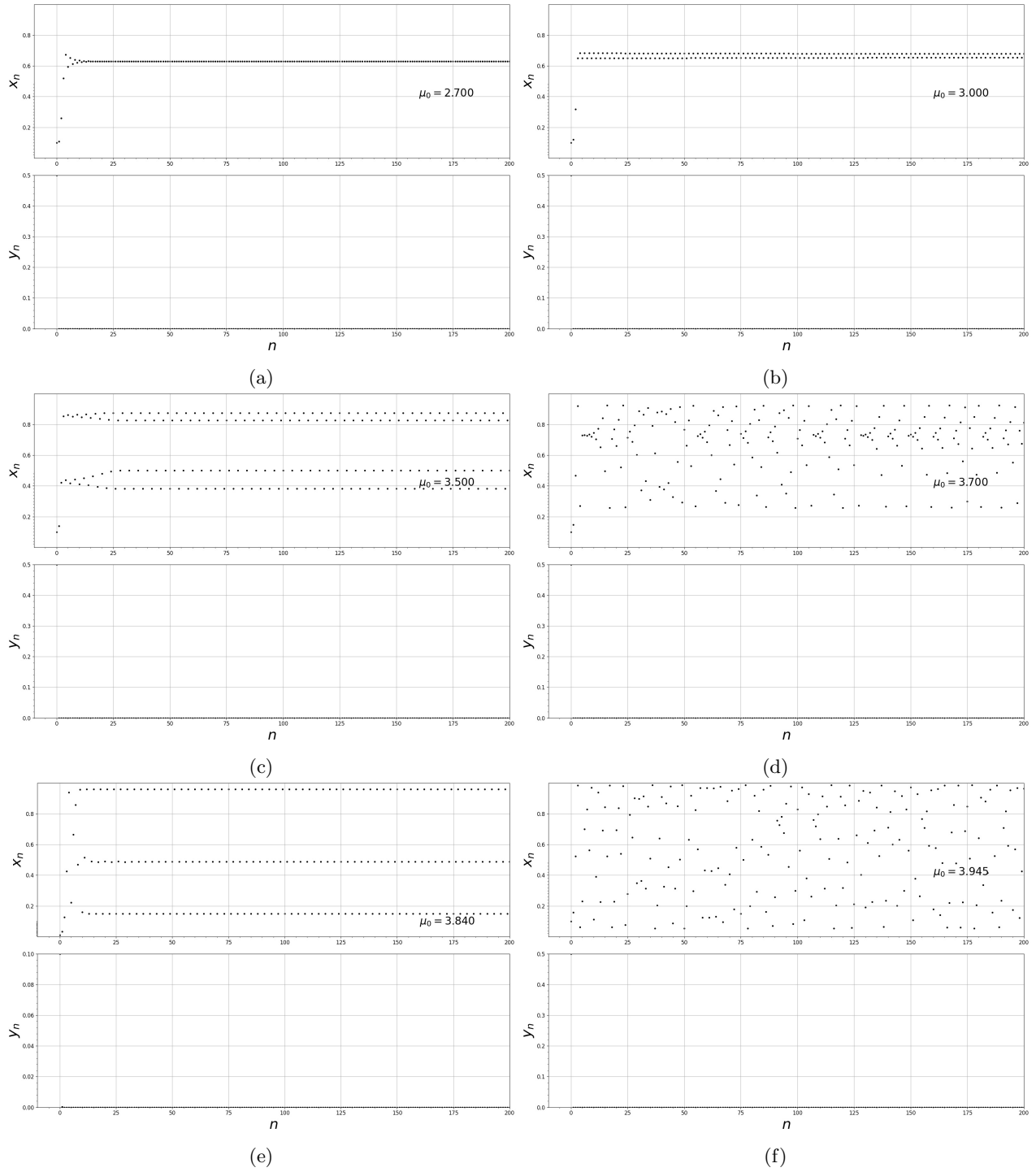


Figure 5: Population vs. iteration of Standard.

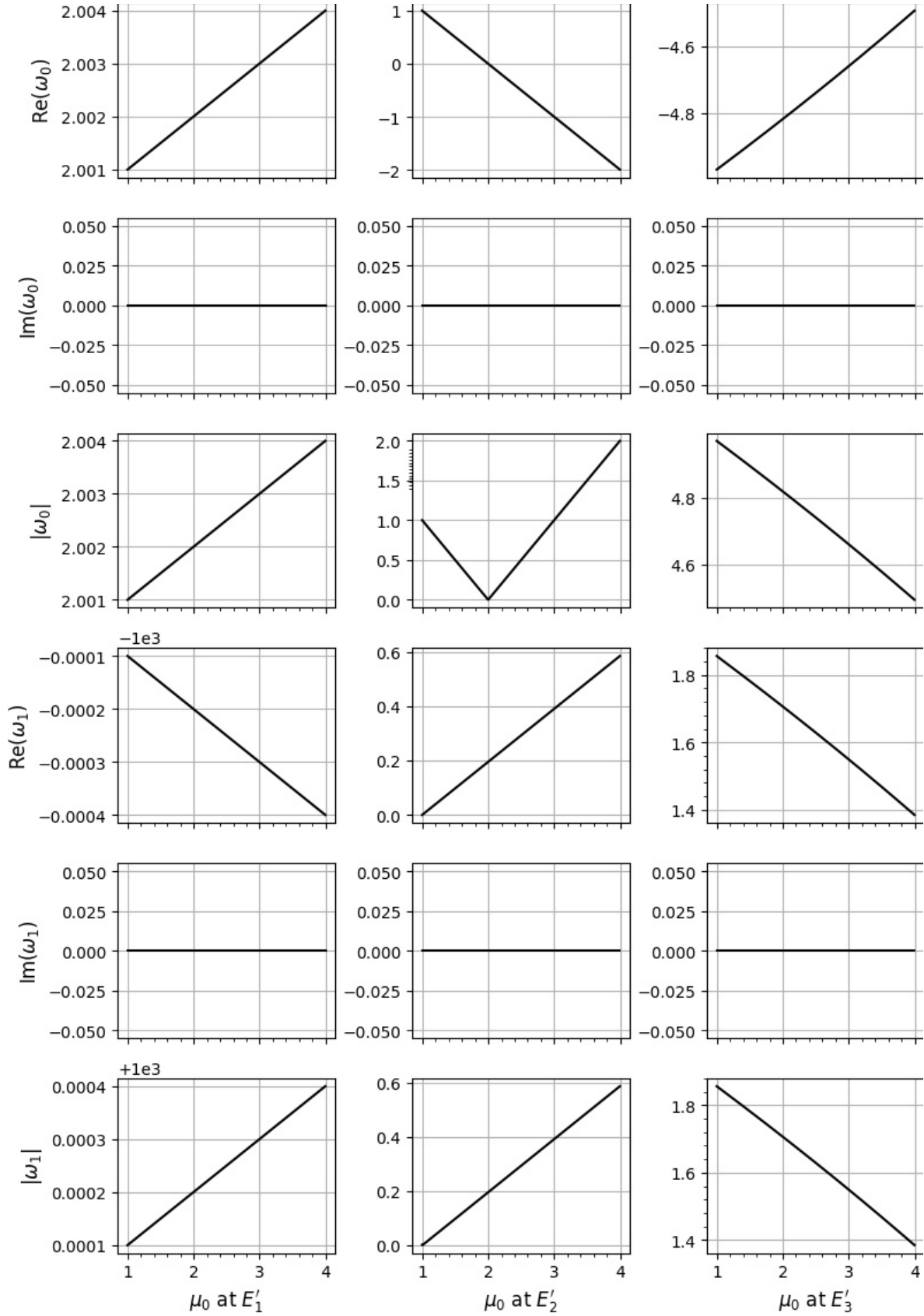


Figure 6: Absolute values of eigenvalues vs. growth rate at fixed points for Standard. We observe that  $E'_2$  is non-hyperbolic at  $\mu_0 = 1$  and 3, while  $E'_3$  is non-hyperbolic at  $\mu_0 = 3.75$ .

### 3.4 Extinction

Figure 7a shows the bifurcation diagram of **Extinction**. There is a flip bifurcation for  $x$  around  $\mu_0 \approx 2.99$ . More explanation will be given for the shaded regions between  $3.165 < \mu_0 < 3.434$  for  $x$  and  $3.10 < \mu_0 < 3.343$  for  $y$ , which are not chaos regions. Subsequently, the bifurcation diagram shows that the population returns to Normal for both  $x$  and  $y$ , and represents pleasant conditions of predictable values before  $x$  enters the 3-cycle, at  $\mu_0 \approx 3.828$  as in Standard, where  $y$  drops to zero cliff fall at  $\mu_0 \approx 3.824$ , manifesting the occurrence of extinction for the predator while the prey is around the 3-cycle state where the onset of chaos is around the corner. Fortunately, there could still be few small chances for the predator to survive at  $(\mu_0, y) = (3.845, 0.219)$ ,  $(3.887, 0.226)$  and  $(3.897, 0.228)$ , where we can see that three isolated fixed points appear with vertical tails. When the prey becomes fully chaotic, the predator population reduces back to zero dramatically again and never has any further opportunity to rise back. This astonishing phenomenon, called *chaotic extinction*, could be the most profound finding of the study, which states that prey in chaos generated by overpopulation of the predator would erase the entire predator species.

Figure 7b shows the Lyapunov exponents for **Extinction** that are similar to those in Figure 3b, except for the regions at  $3.0 < \mu_0 < 3.18$  and  $\mu_0 > 3.86$ , the former showing a bum by Eq.(40), which is also the same region for the prey to be in the 2-cycle, and the latter presenting chaos for  $x$  and extinction for  $y$ .

Figure 8 shows the iteration of the **Extinction** population. As we can see, the flip bifurcation starts at  $\mu_0 = 3.000$  as in Figure(8a), while in Figure(8b) the two fixed points collide and after transient states ( $n > 200$ ), they tend to merge into a single fixed point. We further demonstrate that at  $\mu_0 = 3.500$  in Figure(8c), after transient ( $n > 175$ ), bifurcation collapses to the 1-cycle. Furthermore, the 3-cycle opens in  $x$  at  $\mu_0 = 3.84$ , as indicated in Figure(8d), with extinction of  $y$  at exactly the same time. However, the sunlight of survival for  $y$  is shed in the window at  $\mu_0 = 3.845$ , as shown in Figure(8e), where the two species may still exist in a predictable population.

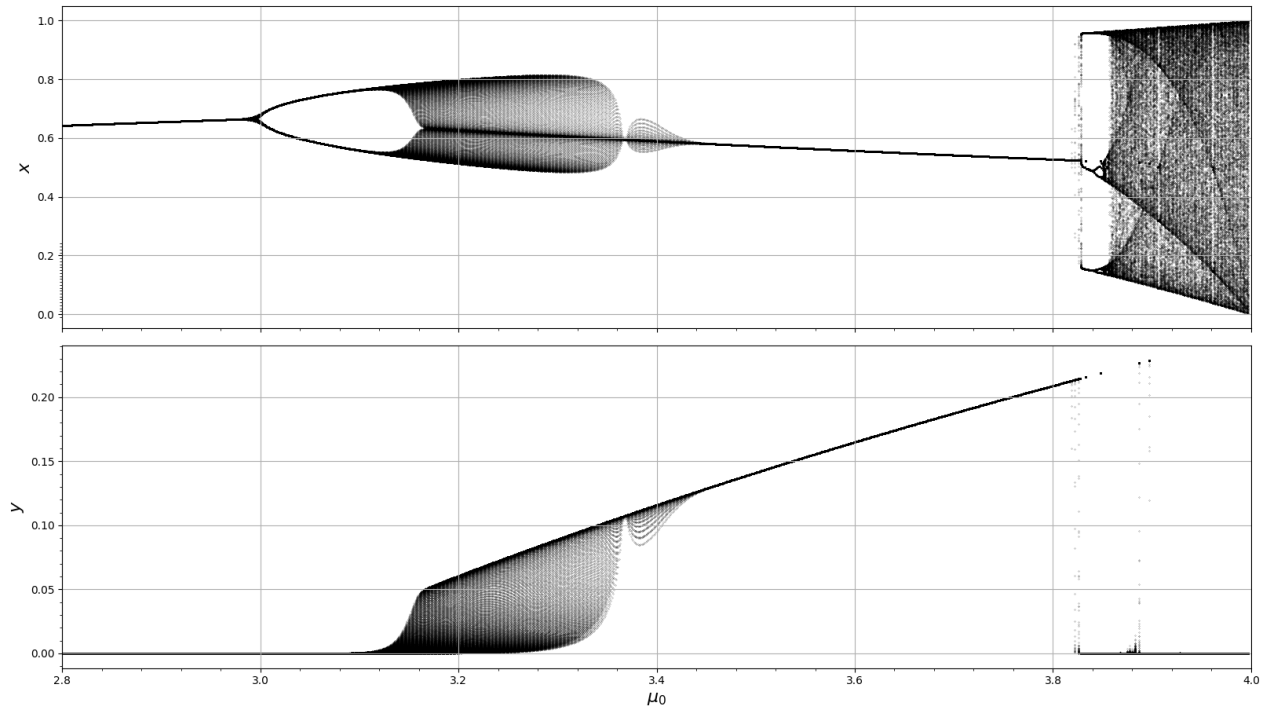
One may argue that since the value  $\beta = 0.001$  is relatively small, our system could simply reproduce that of Danca et al.[28]. However, this is not completely true. For one thing, the parameters  $\mu_1$  and  $\nu_1$  depend on  $\mu_0$  with the help of Hypothesis H<sub>2</sub>. This hypothesis causes the predator to die out very quickly, under certain  $\mu_0$ , within only a few iterations, corresponding to a short time, and leads to an abrupt drop of the predator population shown in Figure 8f, which portends the extinction of predators in the chaos of prey in Figure 7a. In contrast, Danca et al. also pointed out a similar scenario of extinction after thousands of iterations because their system omitted the term  $-\nu_0 y_n(1 - y_n)$ , therefore they cannot see the extinction phenomenon in the bifurcation diagram directly as in our study.

The stability of fixed points may also be examined in Figure 9. The figures in the first column show that  $E'_1$  is a source, since both eigenvalues have absolute values greater than 1. In the second column, we see that  $E'_2$  changes its stability from a sink to a source when  $\mu_0$  varies at 3, at which a flip bifurcation occurs; while,  $E'_3$  changes from source to sink at  $\mu_0 = 3$ .

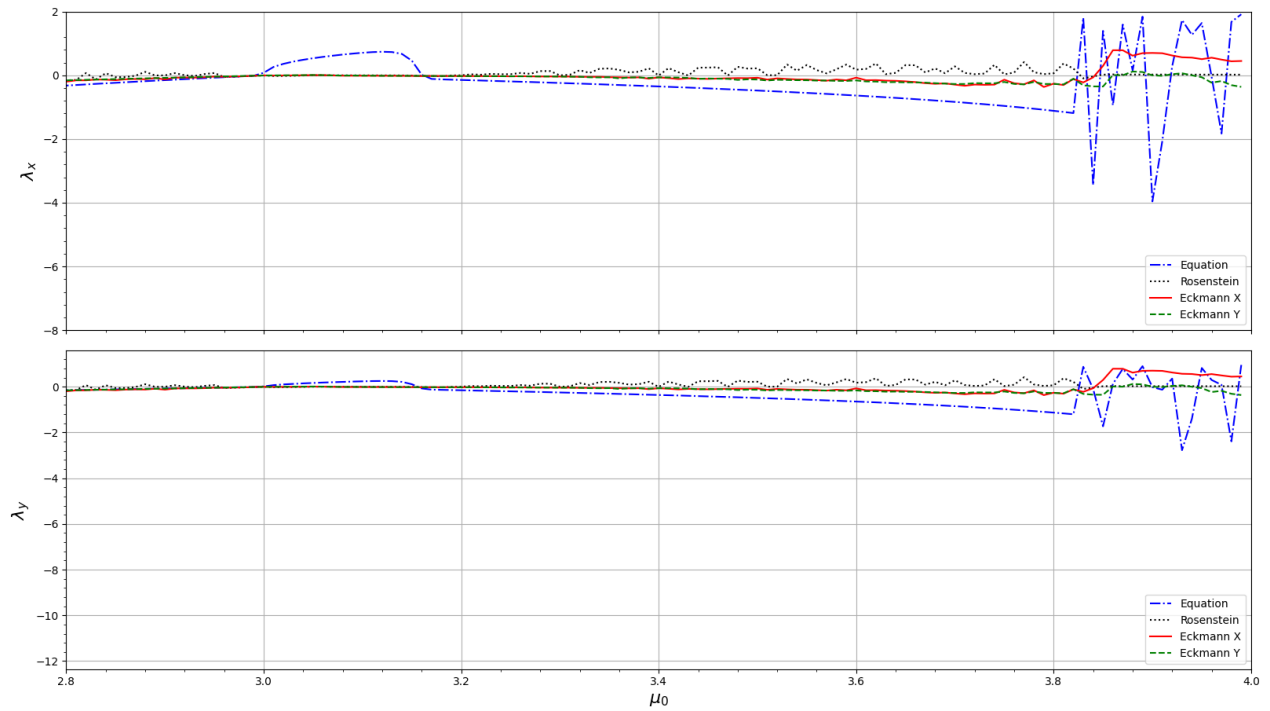
Figure 10 shows a three-dimensional phase portrait with varying  $\mu_0$  of **Extinction**, viewed along the elevation angle  $40^\circ$  and the azimuthal angle  $20^\circ$ . Now a clearer idea of the shaded areas is manifested within  $3.165 < \mu_0 < 3.434$  for  $x$  and  $3.10 < \mu_0 < 3.343$  for  $y$  in Figure 7a, which is quasi-periodic, forming a shape resembling a butterfly wing, subtending to the  $(x, \mu_0)$  plane where  $y$  is extinct.

Figure 11 represents the figures zoomed in within  $3.8 \leq \mu_0 \leq 4$  of the comparisons between **Standard** (in Figure 11a) and **Extinction** (in Figure 11b – d) with different values  $\gamma$  as indicated in each figure. A three-period window of **Standard** within  $3.83 < \mu_0 < 3.86$  in  $x$  is clearly shown in Figure 11a, with  $y$  relatively small (also compared to Figure 4a). As shown in Figures 11b – d, **Extinction** breaks the chaos region before the three-period window (see Figure 11a), making a predictable  $x$  value. On the other hand, the bifurcation diagrams for  $x$  in all subfigures are relatively very similar relative to fine structures, such as supertracks, after the three-period windows. This means that **Extinction** of  $y$  does not influence  $x$  after the three-period window. Finally, a very interesting phenomenon is observed within the three-period window in Figure 11b – d. As we can see, within  $3.825 < \mu_0 < 3.850$ , near the middle of the three-period window, there are some isolated orbitals for  $x$ , and we can find exactly the same orbitals at the same  $\mu_0$  in the corresponding  $y$ . For example, in Figure 11(b), there are five isolated orbitals near the center of the three-period window in  $x$ , and we can find exactly the same number of isolated orbitals at the corresponding  $\mu_0$  for  $y$ . Furthermore, closer inspection reveals that for the residual orbitals of  $y$  in **Extinction**, there are always counterparts in  $x$ . Despite the orbitals before the three-period window in  $x$ , the rest are cloaked by the chaotic region and cannot be seen obviously.

Figure 12 shows comparisons of the predator population ( $y$ ) of **Extinction** for the three values  $\beta = 0.001$ ,  $0.002$  and  $0.003$  with the range  $3.8 < \mu_0 < 4.0$ . In general, the survival population of the predator is very close for different values of  $\beta$ . But there is still some minor difference. Careful analysis shows that increasing  $\beta$  causes a reduction in the number of survival orbitals of the predator, which, not surprisingly, means that increasing the death rate of the predator would diminish the possibility of survival of the predator in the era of **Extinction**. However, if we increase  $\beta$  further, for example  $\beta \geq 0.003$ , **Extinction** phenomenon cannot hold. This counterintuitive result could infer that chaotic extinction cannot occur with a slightly higher death rate of the predator.



(a)



(b)

Figure 7: Bifurcation diagram and Lyapunov exponents of Extinction.

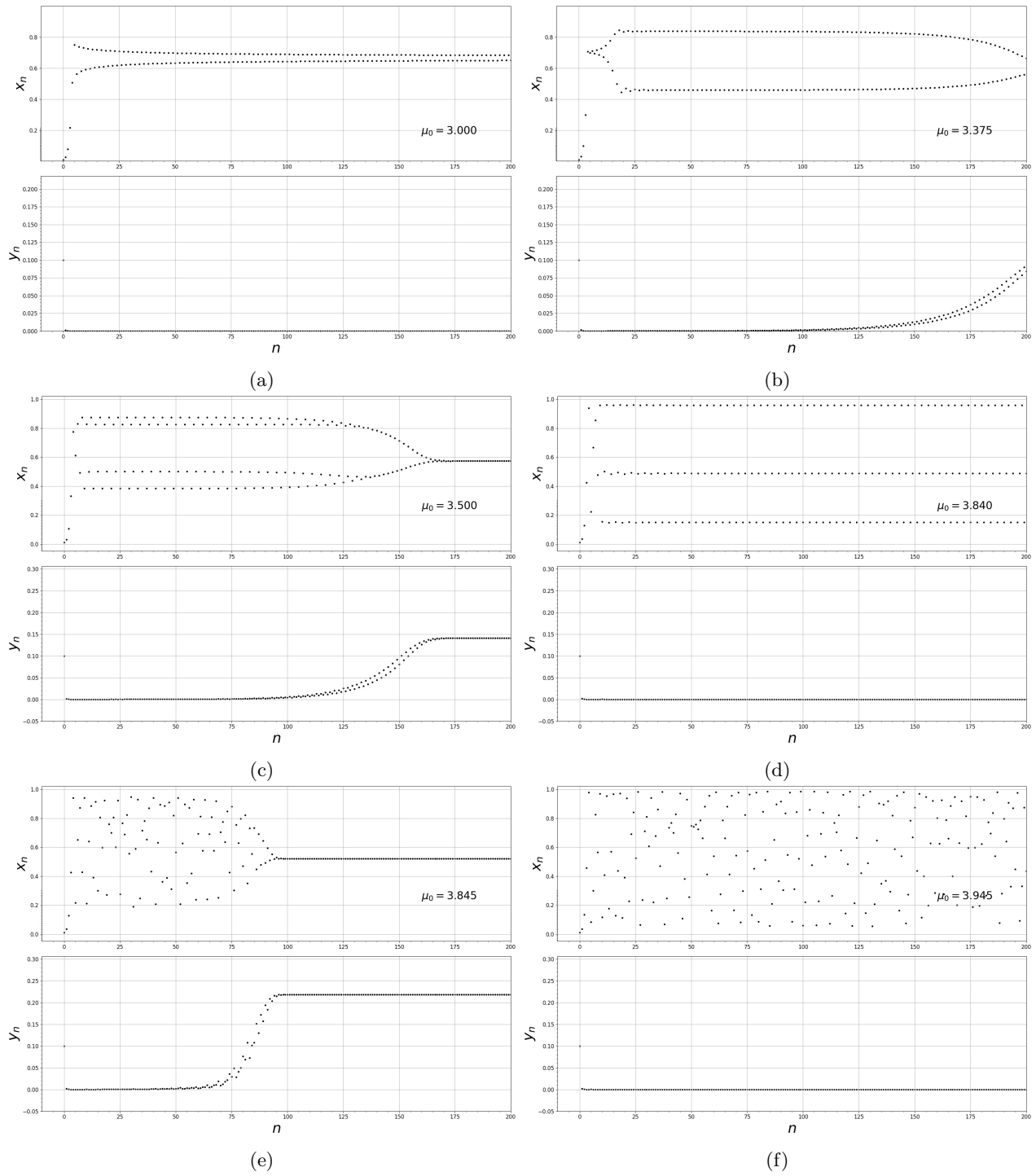


Figure 8: Population vs. iteration of Extinction.

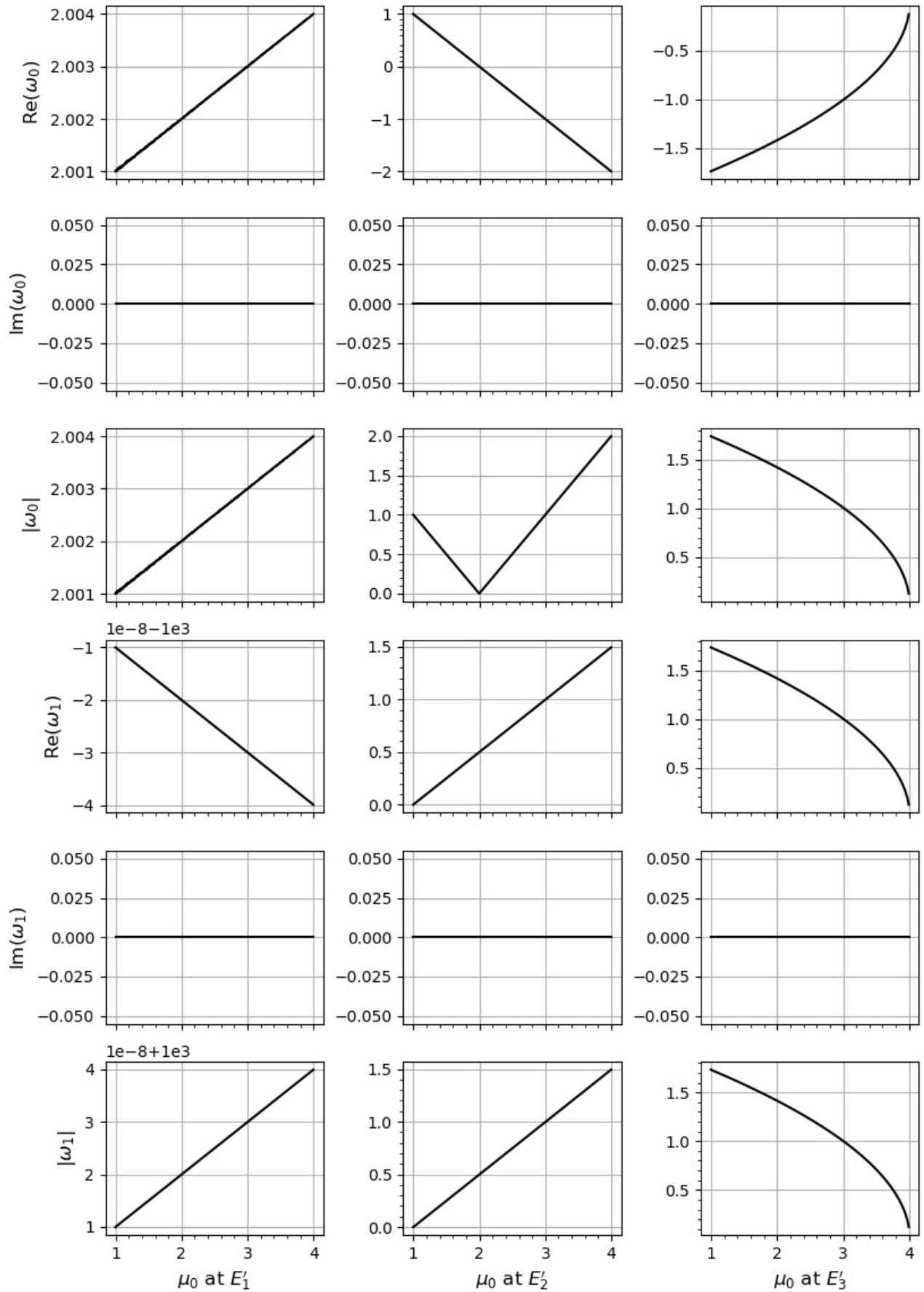


Figure 9: Absolute values of eigenvalues vs. growth rate at fixed points for Extinction. From the figures in the first column, it is clearly shown that  $E_1'$  is a source. Also, at  $\mu_0 = 3$  where flip bifurcation occurs,  $E_2'$  changes its stability from a sink to a source, while  $E_3'$  from source to sink.



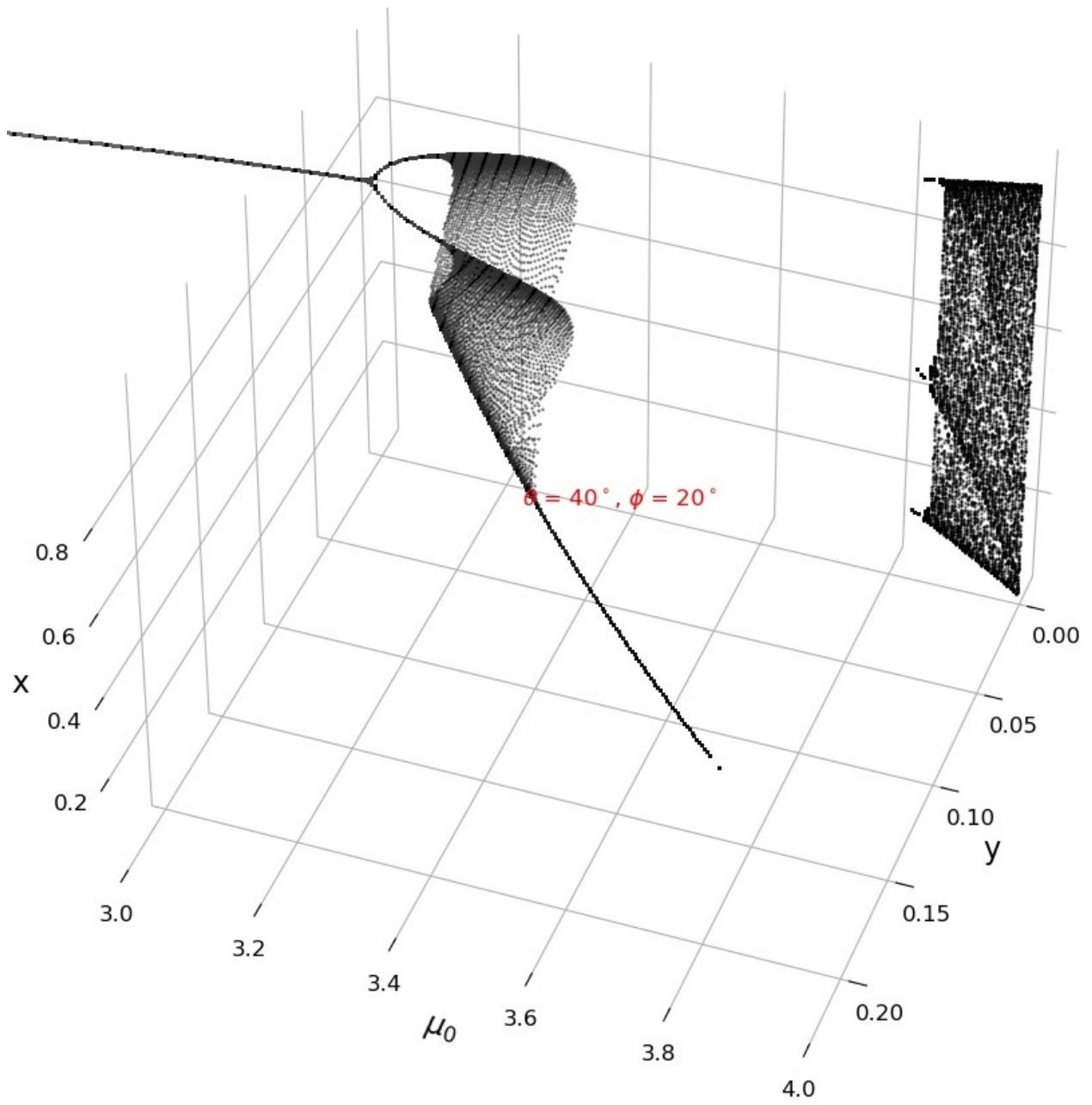


Figure 10: 3D phase portrait of Extinction viewed at elevation  $40^\circ$  and azimuth  $20^\circ$ .

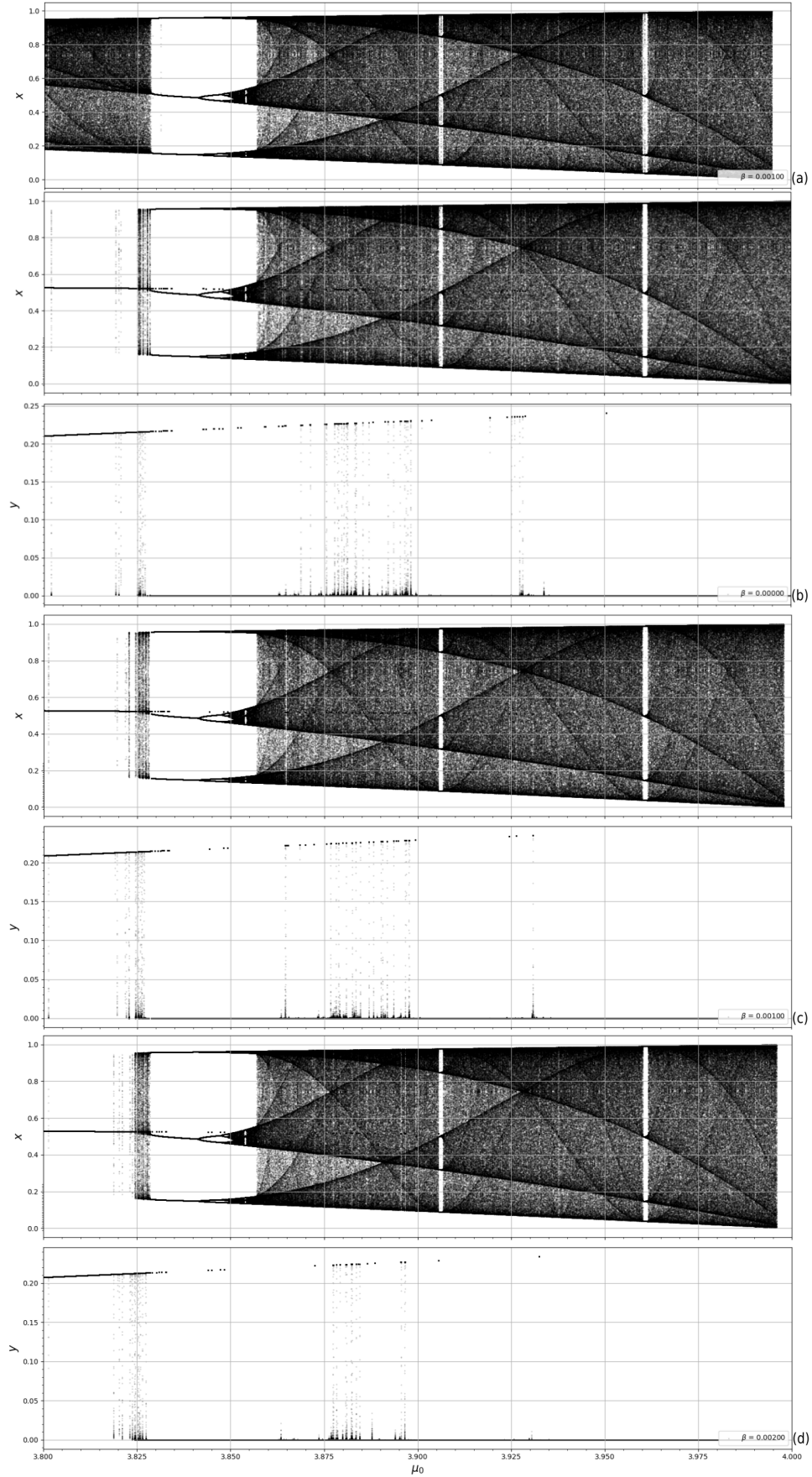


Figure 11: Comparison between Standard and Extinction. Figure 11a, Standard. Figure 11b, Extinction with  $\beta = 0.000$ , Figure 11c with  $\beta = 0.001$ , and Figure 11d with  $\beta = 0.002$ .

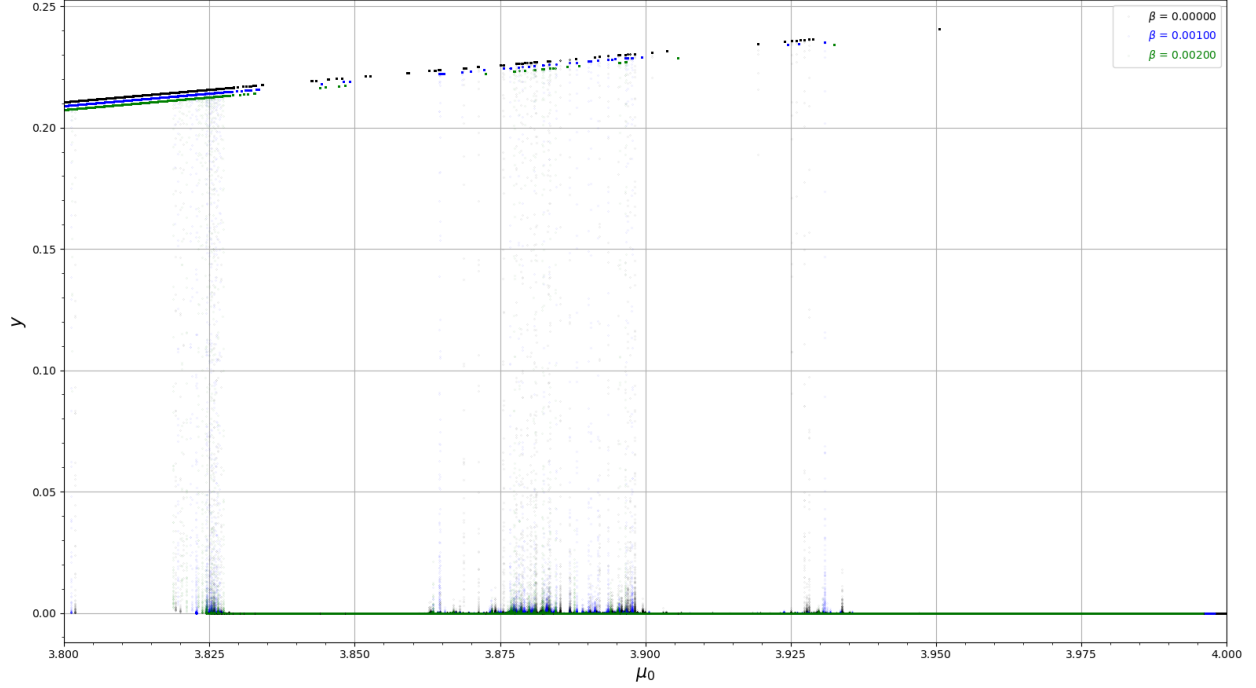


Figure 12: Comparison of  $\beta$  values for the predator population  $y$  of Extinction within  $3.8 < \mu_0 < 4.0$ .

### 3.5 Vorticella

After  $\gamma > 0.694$ , the bifurcation type is Vorticella, named because of its appearance. When  $\mu_0 < 2.0$ ,  $x$  grows steadily without  $y$ . In the presence of the predator, the population of the prey starts to decrease. Both species show a normal population before  $\mu_0 = 3.195 \approx 3.2$ , at which point we classify a Neimark-Sacker bifurcation, as shown in Figure 13a. Figure 13b shows its Lyapunov spectrum. All four algorithms barely show positive spectra for  $x$  and  $y$  before  $\mu_0 = 3.195 \approx 3.2$ . On the contrary, after  $\mu_0 = 3.195 \approx 3.2$ , four algorithms show positive and negative values in the Lyapunov exponents, where the system goes into chaos.

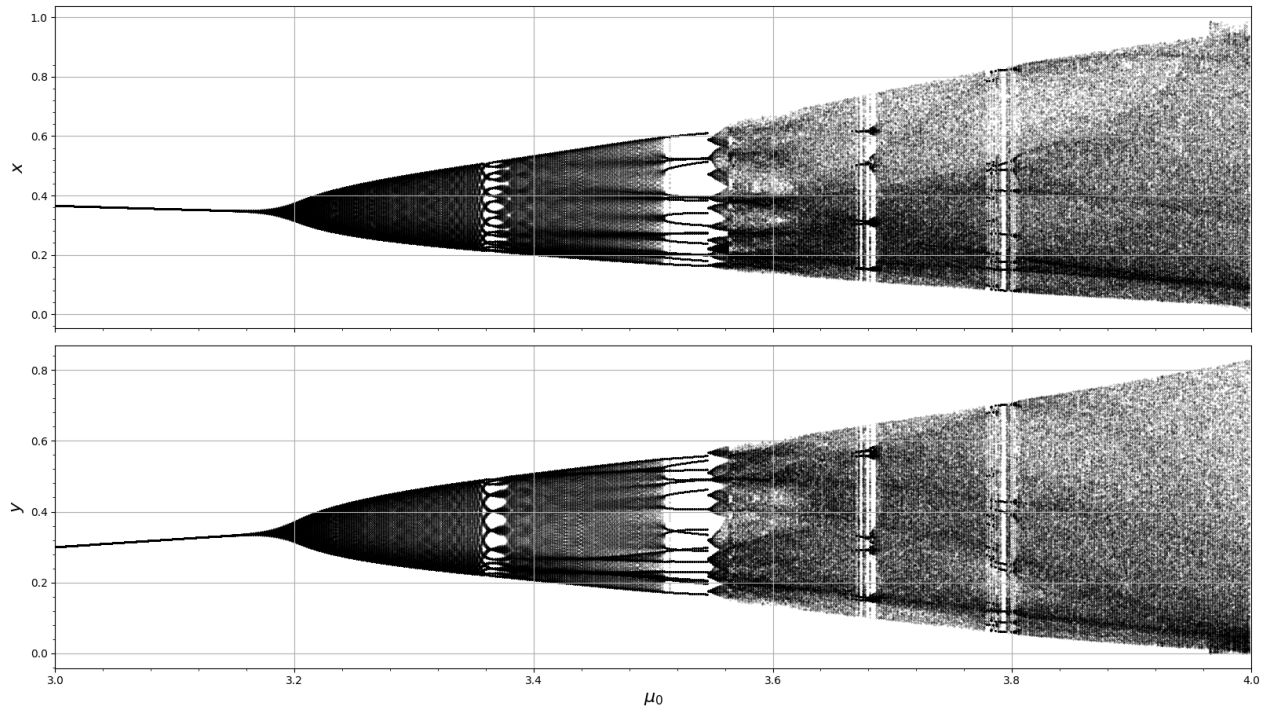
The first row of Figure 14 shows the eigenvalues of  $E'_1$ , both of which have zero imaginary parts, with absolute real parts greater than 1, showing that  $E'_1$  is a source. A similar analysis may also be performed on  $E'_2$ , as shown in the second column of Figure 14. For  $1 < \mu_0 < 2$ ,  $E'_2$  is a sink and turns from a sink to a saddle at  $\mu_0 = 2.1$ , where it is a non-hyperbole ( $\omega_0 \approx 0.166$  while  $\omega_1 = 1$ ). Within  $2.1 < \mu_0 < 3$ ,  $E'_2$  is a saddle, and it turns from a saddle to a source at  $\mu_0 = 3$ , where it is a non-hyperbole ( $\omega_0 = 1$  while  $\omega_1 \approx 1.867$ ). After  $\mu_0 > 3$ ,  $E'_2$  is a source. Finally, the third column in Figure 14 shows that the Neimark-Sacker bifurcation occurs at  $\mu_0 = 3.195 \approx 3.2$ , with coordinates  $(0.346, 0.339)$  in the phase portrait, as shown in Figure 15c due to the following facts: first,  $\omega_0$  and  $\omega_1$  are complex conjugates with modulus 1, and second, as  $\mu_0$  varies between 3.2 from smaller to larger value, the topological type of  $E'_3$  changes from a sink (stable) to a source (unstable)[19].

Hu et al. [10] found a similar bifurcation diagram that was identified as the Hopf bifurcation. However, the criteria for Hopf bifurcation in the two-dimensional system include that the two eigenvalues are purely conjugate imaginary pairs with zero real part[43]. Since Figure 14 shows that  $\omega_1$  has a nonzero real part, our Vorticella cannot be a Hopf bifurcation.

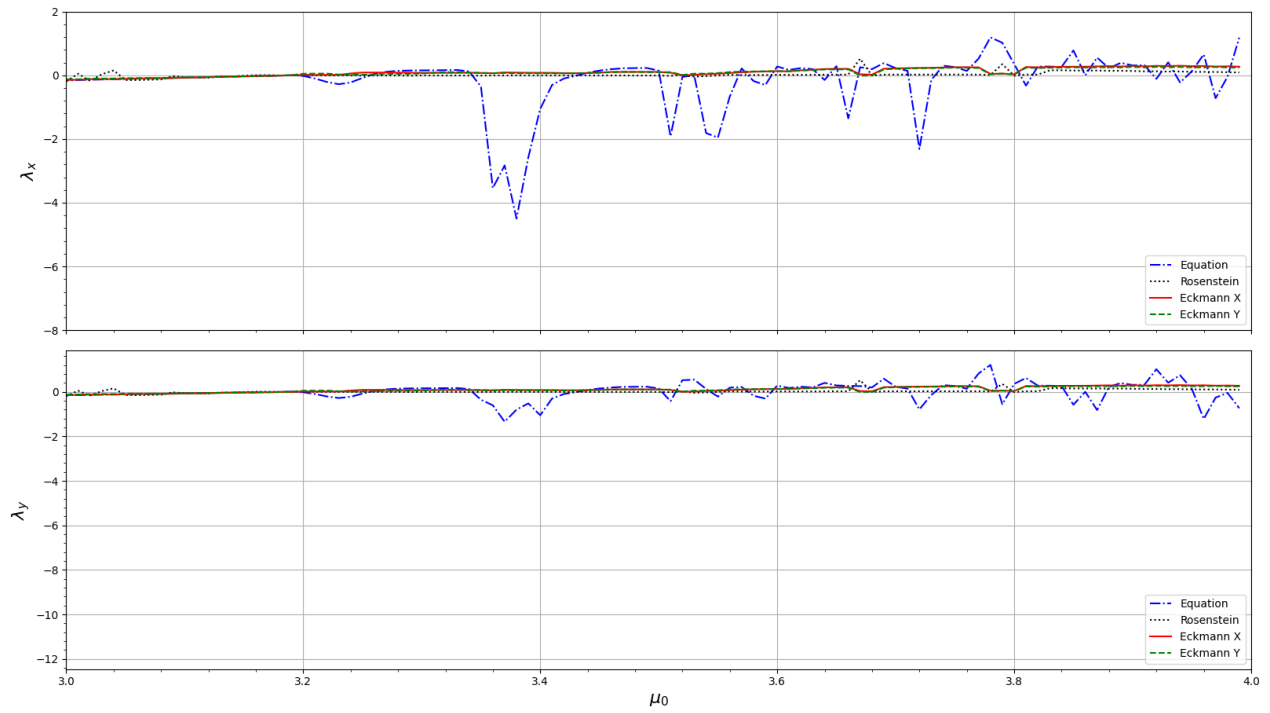
Figure 15 shows some interesting phase portraits in this case. Figure 15a shows a star with  $\mu_0 = 3.055$ , and Figure 15b shows a spiral with  $\mu_0 = 3.150$ , both of which have counterclockwise vector flows spiraling into the fixed point (sink). However, when the Neimark-Sacker bifurcation occurs at  $\mu_0 = 3.195 \approx 3.2$  as shown in Figure 15c, whose stability cannot be determined by linearization and we have to exploit center manifold of mappings, a limit cycle appears and divides the phase portrait into two regions. At  $\mu_0 = 3.310$  (Figure 15d), inside the limit cycle, the vector flow is unstable because the fixed point, represented by the read cycle, is an unstable source, while outside the limit cycle, the vector flow is still stable spiraling toward

the edge of the limit cycle. Before chaos, there are attractor islands that spread around the fixed point (source), as we can see in Figure 15*e*. After that, the phase portrait shows chaos, as in Figure 15*f*. Similar results were found in Danca et al.[28] and Song [44].

It is much more interesting to show the phase portrait in three dimensions, with  $\mu_0$  varying as another axis. In Figure 16, we clearly see that within  $3.2 < \mu_0 < 3.4$ , the phase portraits are loops, although they appear blacked in the corresponding region in the bifurcation diagram (Figure 13*a*.) Within the range  $3.4 < \mu_0 < 3.6$ , there is a phase portrait consisting of attraction islands. After  $\mu_0 > 3.6$ , the phase portraits demonstrate chaos regions with boundaries delimited by black curves. The figure shows that it is important to keep in mind that even if there is a black region in the bifurcation diagram, the system may not exhibit chaos because the black region just exhibits a loop in a higher-dimensional space.



(a)



(b)

Figure 13: Bifurcation diagram and Lyapunov exponents of Vorticella.

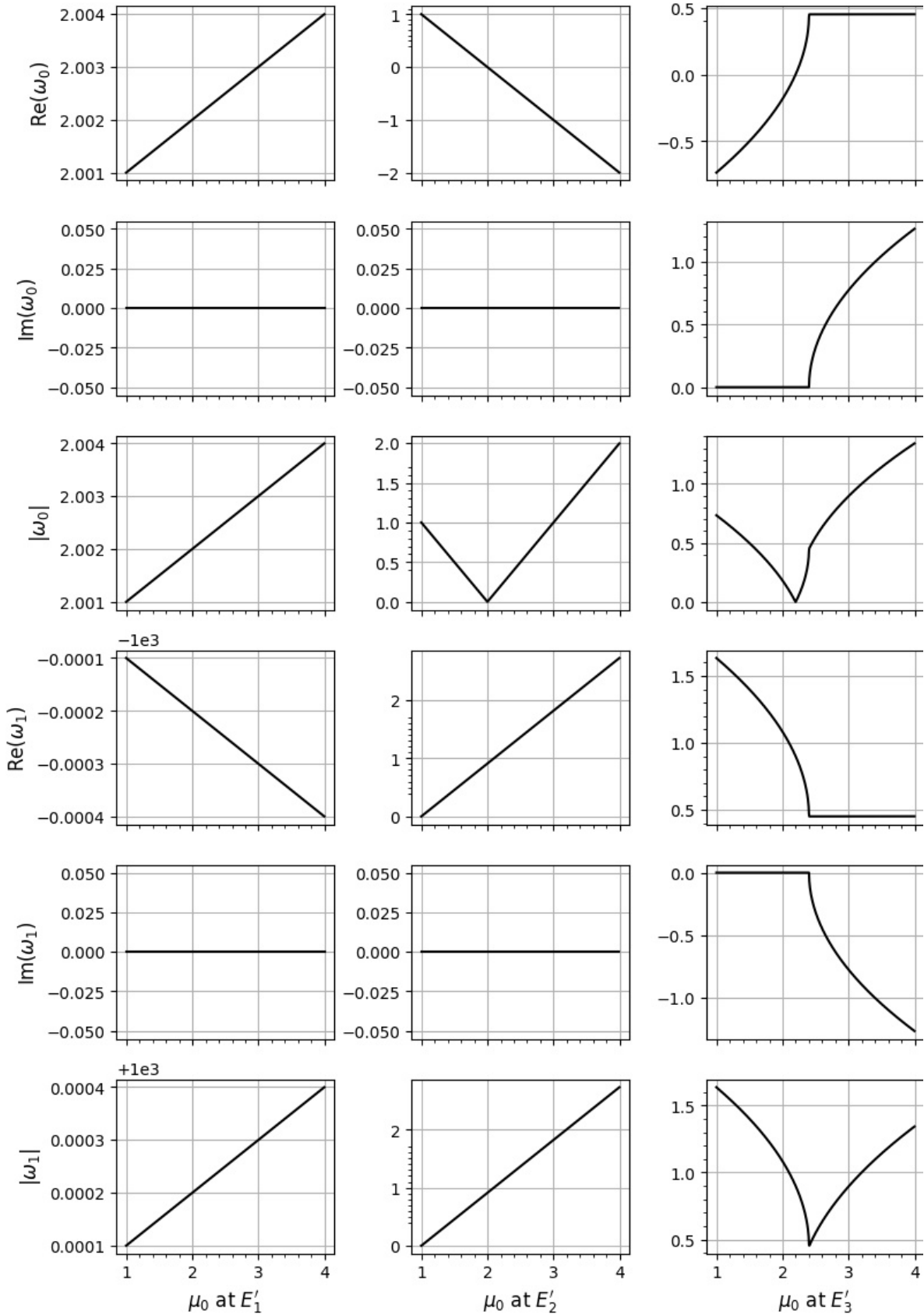


Figure 14: Absolute values of eigenvalues vs. growth rate at fixed points for Vorticella. We observe that  $E'_1$  is always a source.  $E'_2$  is a sink when  $1 < \mu_0 < 2.1$ , a saddle when  $2.3 < \mu_0 < 3$ , and a source when  $3 < \mu_0 < 4$ . In addition,  $E'_2$  is a non-hyperbolic at  $\mu_0 = 2.1$  and  $3$ . For  $E'_3$ , the Neimark-Sacker bifurcation occurs at  $\mu_0 = 3.195 \approx 3.2$ .

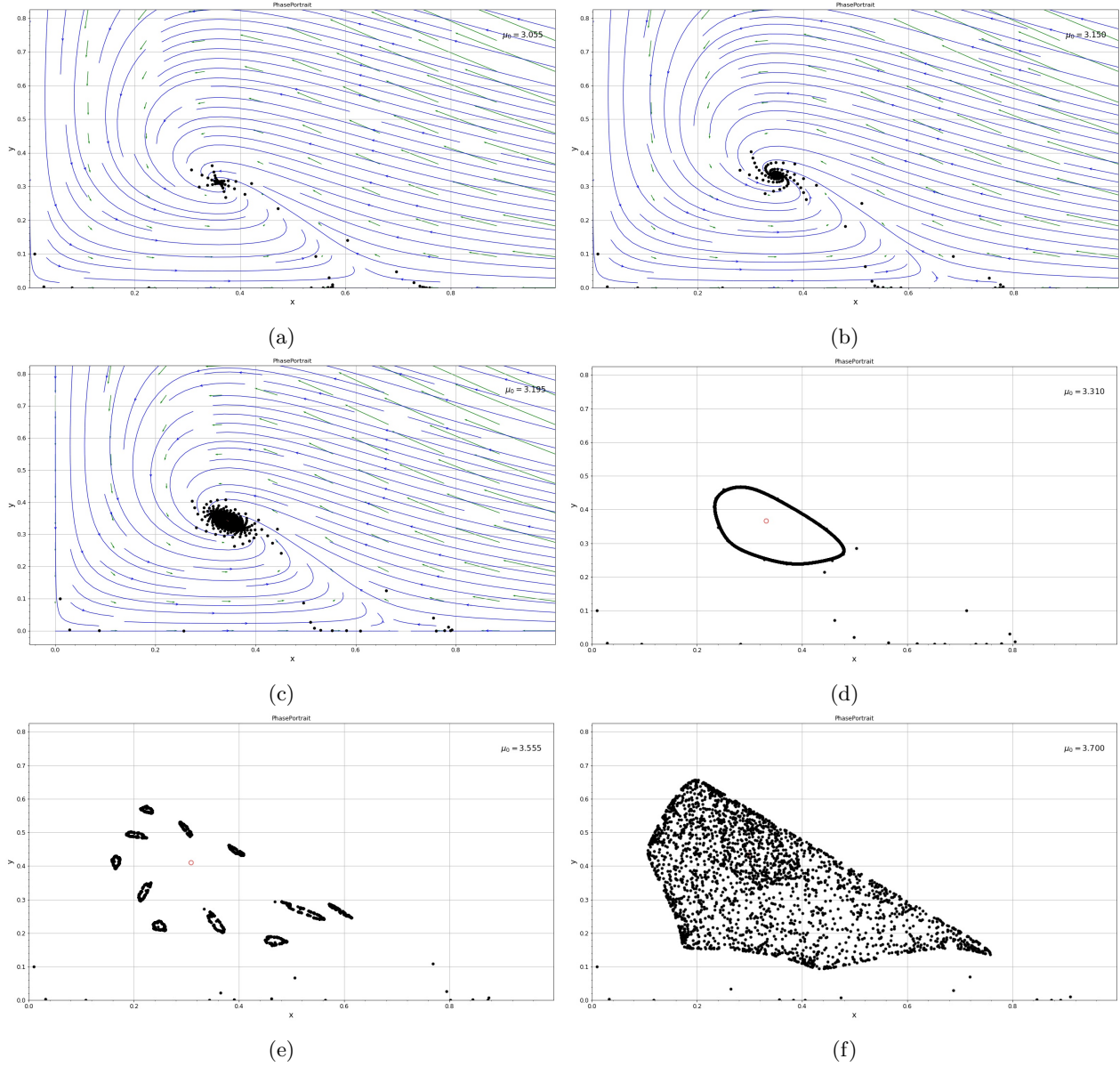


Figure 15: Some outstanding phase portraits of Vorticella.

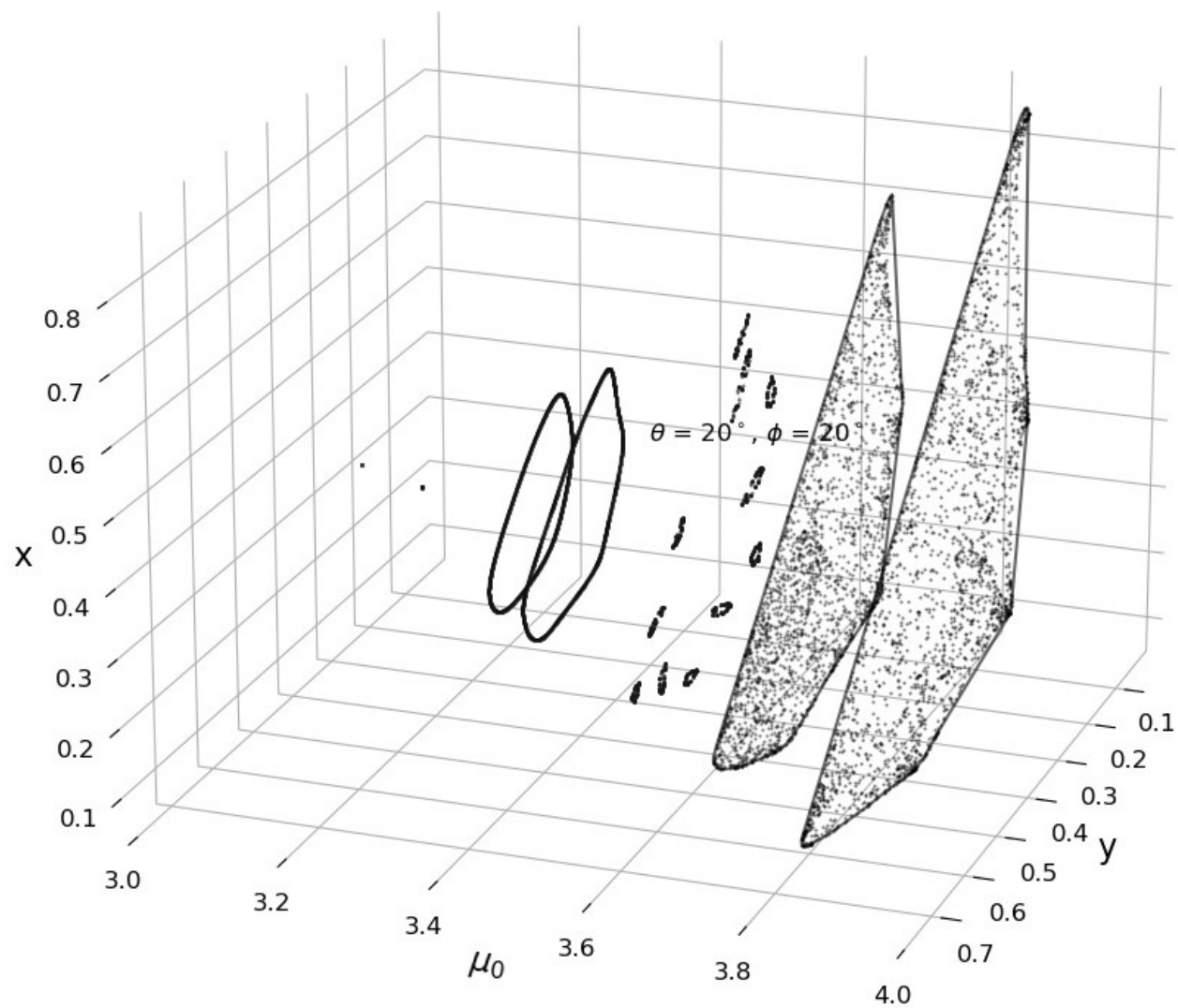


Figure 16: Neimark-Sacker



## 4 Conclusions

We successfully built up a discrete-time model of two-dimensional mapping that resembles features of differential Lotka-Volterra Equations. We studied the topological types of fixed points and found that fascinating feather-like structures were formed around limit circles pierced through by the axis of fixed points in the phase portraits and phase-space diagrams under various growth rates with Neimark-Sacker bifurcation. We further divided our dynamical systems into four categories depending on different shapes of bifurcation diagrams. **Normal**, **Standard**, **Vorticella**, **Extinction**, and **Vorticella**. In each case, we study the stability and topological types of the fixed points using criteria discussed in **Lemma 1**. In addition to plotting the population vs. iteration, we also calculated Lyapunov exponents both by Jacobian eigenvalues of the mapping functions and by the Rosenstein algorithm and Eckmann et al. algorithm. Discrepancies clearly showed that Lyapunov exponents calculated by time-series algorithms may be unreliable within the range of chaos and at low growth rates, as well as when the Lyapunov exponents change dramatically. Furthermore, our model not only regained the logistic mapping 1 D of the prey under zero predator yet with nonzero initial predator population and nonzero interspecies constants, but also showed the normal competitiveness of the prey and the predator without chaos. The quintessence of the current research was that, in addition to the possibility that the prey and predator become chaotic altogether, it is also probable that the predator will go extinct in the chaotic state of the prey. In other words, human overpopulation would cause chaos in natural resources and, ultimately, in return erase the entire human race. Fortunately, even under this difficult circumstance, a slim chance is still left upon us to continue our race under some specific growth rate, as we may see some isolated fixed points remain in the predator bifurcation diagram.

Last but not least, our model may inspire conjecture on other relationships between two quantities coupled with the form of discrete-time difference equations as in our study because mathematically, what we demonstrate is that one of the two quantities may dramatically reduce to zero at the onset state of chaos of the other. Therefore, it could be highly possible that, for example, the superconducting state, which refers to the zero resistance, may be achieved with the chaos of the applied magnetic field. Another possible application may be that we may suppress viruses or pests by triggering the chaotic states of the prey on which the viruses or pests feed for survival.

## 5 Acknowledgment

The authors thank Pui Ching Middle School in Macau PRC for its kindness in supporting this research project.

## References

- [1] Peter Roopnarine, Ecology and the Tragedy of the Commons, Sustainability 2013, 5(2), 749-773.
- [2] Ankit Kumar et al., A Computer-Based Simulation Showing Balance of the Population of Predator and Prey and the Effects of Human Intervention, 2021 IOP Conf. Ser.: Mater. Sci. Eng. 1031 012049
- [3] Cheng Sok Kin et al., Predicting Earth's Carrying Capacity of Human Population as the Predator and the Natural Resources as the Prey in the Modified Lotka-Volterra Equations with Time-dependent Parameters, arXiv:1904.05002v2 [q-bio.PE]. Retrieved via <https://doi.org/10.48550/arXiv.1904.05002>
- [4] K.A. Hasan and M. F. Hama, "Complex Dynamics Behaviors of a Discrete Prey-Predator Model with Beddington-DeAngelis Functional Response", Int. J. Contemp. Math. Sciences, Vol. 7, 2012, no. 45, 2179 - 2195.
- [5] A George Maria Selvam et al., "Bifurcation and Chaos Control for Prey Predator Model with Step Size in Discrete Time", 2020 J. Phys.: Conf. Ser. 1543 012010.
- [6] Boshan Chen and Jiejie Chen, "Bifurcation and Chaotic behavior of a discrete singular biological economic system." Applied Mathematics and Computation, 219(2012) 2371-2386.
- [7] Yong Li et al., "Flip and Neimark-Sacker Bifurcations of a Discrete Time Predator-Prey Model", IEEE Access, Vol. 7, pp. 123430-123435, 2019.
- [8] C. Wang and X. Li, J. Math. Ann. Appl., 422(2015) 920-939.
- [9] X.L. Liu and D.M. Xiau, Complex dynamic behaviors of a discrete-time predator-prey system, Chaos Solitons Fract., 32(2007)80-94.
- [10] Z. Hu, Z. Teng, and L. Zhang, Stability and bifurcation analysis of a discrete predator-prey model with nonmonotonic functional response, Nonlinear Anal. Real World Appl. 12(4)(2011)2356-2377.
- [11] Massimo Cencini, Fabio Cecconi, and Angelo Vulpiani, Chaos: From Simple Models To Complex Systems (Advances in Statistical Mechanics), Wspc; Illustrated edition (September 1, 2009)
- [12] J A Vano, J C Wildenberg, M B Anderson, J K Noel and J C Sprott, Chaos in low-dimensional Lotka-Volterra models of competition, Nonlinearity 19 (2006) 2391-2404.
- [13] Rubin H. Landau, Manuel J. Páez, and Cristian C. Bordeianu, Computational Physics, 2015 WILEY-VCH, pp. 356-357.
- [14] C.M. Evans and G.L. Findley, "A new transformation for the Lotka-Volterra problem", Journal of Mathematical Chemistry 25 (1999) 105-110.
- [15] Dunbar, S. R. (1983). Traveling wave solutions of diffusive Lotka-Volterra equations. Journal of Mathematical Biology, 17(1), 11-32.
- [16] Das, S. and Gupta, P. K. (2011). A mathematical model on fractional Lotka-Volterra equations. Journal of Theoretical Biology, 277(1), 1-6.
- [17] T. Bessoir and A. Wolf, Chaos Simulations, Physics Academic Software, North Carolina State University, Raleigh, NC 27695-8202, USA.
- [18] Pelinovsky, E., Kurkin, A., Kurkina, O., Kokoulina, M., and Epifanova, A. (2020). Logistic equation and COVID-19. Chaos, Solitons & Fractals, 140, 110241.

- [19] A. Mareno, L. Q. English, "Flip and Neimark–Sacker Bifurcations in a Coupled Logistic Map System", *Discrete Dynamics in Nature and Society*, vol. 2020, Article ID 4103606, 14 pages, 2020. <https://doi.org/10.1155/2020/4103606>
- [20] Bo Li, Qizhi He and Ruoyu Chen, "Neimark–Sacker bifurcation and the generate cases of Kopel oligopoly model with different adjustment speed", *Advances in Difference Equations* (2020) 2020:72, <https://doi.org/10.1186/s13662-020-02545-9>.
- [21] Zeraoulia Elhadj and J. C. Sprott, "The effect of modulating a parameter in the logistic map", *Chaos* 18, 023119 (2008).
- [22] Andrey L. Shilnikov and Nikolai F. Rulkov, Origin of Chaos in a Two-Dimensional Map Modeling Spiking-Bursting Neural Activity, *International Journal of Bifurcation and Chaos*, Vol. 13, No. 11(2003), 3325-3340.
- [23] Waqas Ishaque, Qamar Din, Muhammad Taj and Muhammad Asad Iqbal, "Bifurcation and chaos control in a discrete-time predator–prey model with nonlinear saturated incidence rate and parasite interaction", *Advances in Difference Equations* (2019) 2019:28, <https://doi.org/10.1186/s13662-019-1973-z>
- [24] Asifa Tassaddiq, Muhammad Sajjad Shabbir, Qamar Din and Humera Naaz, "Discretization, Bifurcation and Control for a Class of Predator–Prey Interactions", *Fractal Fract.* 2022, 6(1), 31; <https://doi.org/10.3390/fractalfract6010031>
- [25] Abd-Elalim Elsadany, H.A. EL-Metwally, E.M. Elabbasy, and H.N. Agiza, Chaos and bifurcation of a nonlinear discrete prey-predator system, *Computational Ecology and Software*, 2012, 2(3): 169-198.
- [26] Michael P. Hassell, Hugh N. Comins & Robert M. Mayt, "Spatial structure and chaos in insect population dynamics", *Nature* volume 353, pages 255–258 (1991)
- [27] A. A. Berryman and J.A. Millstein, "Are Ecological Systems Chaotic-And If Not, Why Not?", *Trends Ecol Evol.* 1989 Jan;4(1):26-8. doi: 10.1016/0169-5347(89)90014-1.
- [28] Danca, MF., Fečkan, M., Kuznetsov, N. et al. Rich dynamics and anticontrol of extinction in a prey–predator system. *Nonlinear Dyn* 98, 1421–1445 (2019). <https://doi.org/10.1007/s11071-019-05272-3>
- [29] M. T. Rosenstein, J. J. Collins, and C. J. De Luca, "A practical method for calculating largest Lyapunov exponents from small data sets," *Physica D: Nonlinear Phenomena*, vol. 65, pp. 117–134, 1993.
- [30] J. P. Eckmann, S. O. Kamphorst, D. Ruelle, and S. Ciliberto, "Liapunov exponents from time series," *Physical Review A*, vol. 34, no. 6, pp. 4971–4979, 1986.
- [31] A.J. Lotka, "Contribution to the Theory of Periodic Reaction", *J. Phys., Chem.* 14(3), 271–274, 1910.
- [32] V. Volterra, "Variazioni e fluttuazioni del numero d'individui in specie animali conviventi". *Mem. Acad. Lincei Roma.* 2: 31–113, 1926.
- [33] Lotka-Volterra Equation Wikipedia, [https://en.wikipedia.org/wiki/Lotka%E2%80%93Volterra\\_equations](https://en.wikipedia.org/wiki/Lotka%E2%80%93Volterra_equations)
- [34] Immanuel M. Bonze, Lotka-Volterra Equation and Replicator Dynamics: A Two-Dimensional Classification, *Biol. Cybern* 48, 201-221, 1983. Eq 4 in our work has the same form as Eq 2 in this reference.
- [35] Steve H. Strogatz, *Nonlinear Dynamics and Chaos*, p.156, Addison Wesley, 2nd Ed.
- [36] Alan Wolf, Jack B. Swift, Harry L. Swinney and John A. Vastano, Determining Lyapunov Exponents from a Time Series, *Physica* 16D, 285-317, 1985.
- [37] Lorenzo Escot and Julio E. Sandubete Galan, "A brief methodological note on chaos theory and its recent applications based on new computer resources", *Revista: ENERGEIA* (ISSN: 1666-5732) Vol. VII, Núm. 1, 2020, pp. 53-64.

- [38] Schölzel, Christopher. (2019, June 16). Nonlinear measures for dynamical systems (Version 0.5.2). Zenodo. <http://doi.org/10.5281/zenodo.3814723>
- [39] Codes and animations may be retrieved via <https://github.com/weishanlee/LotkaVolterraChaos>
- [40] Stephen T. Thornton and Jerry B. Marrion, Classical Dynamics of Particles and Systems, 5th Ed., CH4, ISBN-10:0534408966
- [41] IGI Global <https://www.igi-global.com/dictionary/flip-bifurcation/11262>
- [42] Herbert Goldstein, Charles Poole, John Safko, Classical Mechanics, 3rd Ed, CH11, ISBN-10:0321188977.
- [43] J. Hale, and H Koçak, Dynamics and Bifurcations. CH 11, Vol. 3, Berlin: Springer-Verlag (1991). ISBN-13: 9783540971412.
- [44] Ning Song, "Bifurcation and Chaos of a Nonlinear Discrete-Time Predator-Prey Model Involving the Nonlinear Allee Effect", Discrete Dynamics in Nature and Society, vol. 2023, Article ID 5475999, 32 pages, 2023. <https://doi.org/10.1155/2023/5475999>